Journal of MATERIALS RESEARCH

Review
DOI:10.1557/s43578-022-00868-9

A review of plasma-assisted deposition methods for amorphous carbon thin and ultrathin films with a focus on the cathodic vacuum arc technique

Anurag Roy[1], Shengxi Wang[1], Kyriakos Komvopoulos[1,a]

[1] Department of Mechanical Engineering, University of California, Berkeley, CA 94720, USA
[a)] Address all correspondence to this author. e-mail: kyriakos@me.berkeley.edu

Received: 30 September 2022; accepted: 2 December 2022; published online: 5 January 2023

Amorphous carbon (*a*-C) films have garnered significant attention over the past few decades, principally due to their remarkable thermophysical properties, strong adherence to various materials, and good chemical inertness. These intrinsic characteristics of *a*-C films have led to their use as protective overcoats in numerous applications, such as hard-disk drives, microelectromechanical systems, and biomedical implants. The significant thinning of *a*-C films to a few nanometers, dictated by rapid advances in device miniaturization and compactness, motivated the development of thin-film deposition methods that preserve important film attributes like uniformity, strength, and structural stability. This article provides a comprehensive assessment of the most effective deposition techniques for synthesizing ultrathin films, particularly *a*-C films due to their wide application range as protective overcoats in contemporary technologies, state-of-the-art microanalysis methods for ultrathin films, and the technology challenges that must be overcome for CVA to capture a bigger share of the thin-film technology marketplace.

Introduction

Amorphous carbon (*a*-C) films have been garnering considerable attention mainly because of their unique set of properties, such as low coefficient of friction, high hardness, good wear resistance, excellent biocompatibility, novel optical and electrical characteristics, and high chemical inertness [1–9]. Except of the optical/electrical properties and biocompatibility, all of the former attributes can be traced back to the relatively high content of tetrahedral (sp^3) carbon atom hybridization. For example, a very high sp^3 content (~86%) has been reported for hydrogen-free *a*-C films [10, 11], which is a radical departure from the previous notion that carbon films with such high sp^3 content that are devoid of hydrogen do not exist, especially in non-crystalline structure form [12], whereas other research [10, 11] postulated the structure of these films is similar to that of *a*-Si and *a*-Ge.

Various techniques [1, 2, 13–22] have been developed to synthesize thin *a*-C films, including plasma-enhanced chemical vapor deposition (PECVD), ion beam sputtering, plasma immersion ion implantation and deposition (PIIID), radio-frequency (rf) and magnetron sputtering, pulsed laser deposition (PLD), pulsed laser ablation (PLA), and cathodic vacuum arc (CVA). *a*-C and *a*-C:X (X = H, N, Au, Ag, Cu, Mo, W, Cr, Nb, Pd, Pt, Ti, and MoS_2) films have been used to protect vital components in a wide range of applications, such as magnetic storage, microelectromechanical systems, proton-exchange membrane fuel cells, food storage, solar cells, outer space and aviation, and biomedical implants [2, 6–8, 21, 23–37]. An extensive compilation of other applications of *a*-C and *a*-C:X films besides those mentioned here can be found elsewhere [38]. However, the primary focus of this article is on the usage of plasma-based methods to synthesize ultrathin *a*-C films, with a special emphasis placed on CVA, which can be used in applications where thermal effects are critical, such as heat-assisted magnetic recording (HAMR). Because of their excellent tribomechanical properties, ultrathin *a*-C films have been extensively used as protective overcoats in hard-disk drives (HDDs). Since the actual spacing between the read/write transducer and magnetic media in contemporary HDDs is currently ~5 nm [39, 40], the *a*-C overcoat thickness must be ~2 to 3 nm to allow the HDDs to perform their intended function. Such an extremely small film thickness makes uniform film deposition and characterization challenging, especially when the ultrathin film exhibits a layered structure.

It is well established that *a*-C films synthesized by the CVA method possess a layered cross-sectional structure consisting of three main layers, namely intermixing, bulk, and surface layer [41–44]. Of these three layers, the significantly richer in sp^3-hybridized carbon bulk layer is responsible for the high hardness and excellent tribomechanical properties of these *a*-C films [45]. The impetus to reduce the thickness of the protective *a*-C overcoat in magnetic storage HDDs has been fueled by demands to enhance the storage capacity. This is due to the exponential increase of the magnetic signal intensity with the decrease of the magnetic spacing predicted by Wallace's law [46], which is responsible for the increase of the data storage density in contemporary HDDs to several Tb/in^2 [47–50]. Consequently, the perennial challenge is to reduce the thickness of the *a*-C overcoat without compromising its functionality, structural integrity, and endurance. Moreover, although miniaturization is the ultimate objective in rapidly emerging magnetic storage technologies, the profound thinning of the *a*-C overcoat decreases both the overall sp^3 content [51] and, more detrimentally, the thickness of the protective bulk layer [41, 52, 53], which is mainly responsible for the desired tribo-thermo-mechanical properties and oxidation resistance of *a*-C films synthesized by energetic ion bombardment methods.

The CVA technique has been proven to be one of the most promising methods for depositing sub-5-nm-thick continuous films. This unique capability stems from a host of advantages provided by this method, especially filtered CVA (FCVA), such as low-temperature ultrathin film synthesis, effective plasma manipulation, macroparticle filtering, pulsed substrate biasing, and stable plasma arcing [54, 55]. Although the focus of this article is on the synthesis and characterization of CVA-deposited *a*-C films, co-deposition of various metals to form hybrid *a*-C:M (M = metal) films can be accomplished by dual-cathode/dual-source CVA [56–63] and species-selective biasing [57, 59–61], which are also discussed in this article. A plethora of macroparticle filters have been designed in the course of developing the CVA method, each with its own unique sets of attributes, advantages, and deficiencies, having as the main goal to allow only high quality C^+ ions to reach the substrate surface and filter out any macroparticles expelled from the cathode as a result of the explosive nature of the arcing process. A variety of ingenious tactics have been adopted in designing these filters, including the elimination of the direct deposition (line-of-sight) requirement by using curved ducts, open filters, S-shaped ducts, angled double bends, out-of-plane bends, and magnetic fields imparting a specific radius, depending on the ion charge and ion mass [54, 64–79]. A comprehensive review of various macroparticle filters used in CVA systems can be found elsewhere [80]. The growth of particle-free, ultrathin *a*-C films with the FCVA technique has been demonstrated in several studies [53, 81, 82].

In view of the growing demands for ultrathin *a*-C overcoats, high-resolution characterization techniques were developed to circumvent the limited effectiveness of most traditional microanalysis techniques to probe the composition and structure of nanometer-thick films. To examine the local structure and chemical composition at the micro/nanoscale, several imaging and spectroscopic techniques have been advanced, including X-ray diffraction (XRD) [61, 83–86], nuclear magnetic resonance (NMR) [87–89], X-ray reflectivity (XRR) [90–92], Raman spectroscopy [90, 93–95], electron spectroscopy for chemical analysis performed by X-ray photoelectron spectroscopy (XPS) [14, 42, 96], transmission electron microscopy (TEM) [41, 44, 52, 53, 97–101], and electron energy loss spectroscopy (EELS) [42, 102–108]. These characterization methods enable accurate estimates of the thickness, composition, and structure of ultrathin *a*-C films, particularly tetrahedral (sp^3) and trigonal (sp^2) atomic carbon hybridization fractions. The sp^3 content is of paramount importance because it directly correlates with the thermal, mechanical, and tribological properties, the magnitude of the internal compressive stress, and the corrosion/oxidation behavior of the *a*-C film [45, 109].

Despite significant insight into the room-temperature structure and tribomechanical properties of *a*-C films obtained from previous studies, basic knowledge of the structural stability and tribomechanical properties of *a*-C films at elevated temperatures is relatively limited. Since several cutting-edge technologies depend on the effective operation of a device at elevated temperatures, even more stringent requirements are applicable to the mechanical integrity of *a*-C films. For example, the *a*-C overcoats intended for HAMR HDDs must demonstrate structural stability at a steady-state temperature of 250–350 °C (head) and transient peak temperatures of about 450–650 °C (hard disk), depending on the Curie temperature of the magnetic media. For this reason, thermal annealing studies [81, 110–112] were performed to provide insight into temperature-induced changes in the structure, composition, and thickness of the constituent layers comprising the layered structure of CVA-synthesized *a*-C films.

A design philosophy of durable *a*-C films requires a thorough understanding of the effect of principal deposition parameters on the resulting film nanostructure. Because the design space includes several interdependent input and output parameters, identifying an optimum processing window is critically important. In the case of the FCVA method, for example, independent key input parameters are the ion kinetic energy (controlled by substrate biasing), the ion flux and incidence angle, the amplitude, frequency, and duty cycle of the substrate bias voltage, the cathode and substrate materials, and the deposition time. Output parameters that depend on the former input parameters include the nanostructure (hybridization state), chemical composition, and thickness of the intermixing, bulk, and surface layers

encompassing the *a*-C film, and the overall thickness, surface topography, and tribo-thermo-mechanical properties of the film. Several parametric studies have been carried out to determine the optimum range for these output parameters [17, 52, 53, 97–100, 103, 113–118]. For instance, because the kinetic energy of C^+ ions generated by the arcing process, which is intrinsic to the FCVA technique, is equal to ~ 20 eV [39, 115], the final kinetic energy of C^+ ions arriving at the substrate surface is principally determined by the substrate bias voltage. There are two competing processes affecting deposition, i.e., collision cascades between substrate atoms and impinging C^+ ions, causing locally high pressure gradients, which aid sp^3 hybridization, as well as thermal spikes and thermal relaxation induced by the highly energetic C^+ ions, which are conducive to sp^3-to-sp^2 rehybridization. Thus, tuning the ion kinetic energy [56, 113] in conjunction with other important input parameters is critical to tailoring the structure, composition, tribomechanical properties, and thermal stability of protective ultrathin *a*-C films.

To further enhance the protective performance of *a*-C overcoats, an ultrathin underlayer may be used as an adhesion layer and/or oxidation and element diffusion barrier. Thermal effects may lead to carbon diffusion into the substrate material, affecting the intended functionality of the device. For instance, diffusion of carbon from the *a*-C overcoat into the Au near-field transducer (NFT) or the FeCo write pole (WP) may render these vital components of the magnetic head dysfunctional. Moreover, because *a*-C does not adhere well onto metallic substrates, there is a persistent quest for an underlayer exhibiting good adhesion characteristics to both *a*-C and metals. In general, Si-based underlayers have been reported to serve this need. For instance, recent studies [81, 82, 119–126] have shown that a SiN_x underlayer can effectively play the dual role of adhesion layer and diffusion barrier. Layered overcoats consisting of an ultrathin *a*-C outer layer and an ultrathin underlayer consisting of a high-density material, possibly alloyed with a refractory element to further enhance its thermal stability, demonstrate a high potential as protective media for precious metallic elements exposed to elevated temperatures, such as the NFT and WP of HAMR HDDs. Furthermore, composite coatings consisting of carbon interspersed with nanostructures resembling graphene [127] can enhance the tribomechanical characteristics and oxidation/corrosion resistance [128].

The main objectives of this article are to provide a comprehensive overview of plasma-assisted film deposition methods with special emphasis on CVA-deposited ultrathin *a*-C films, and an appraisal of pertinent film characterization methods. Ultrathin *a*-C films are used in various contemporary applications principally due to their unique thermal, mechanical, and tribological characteristics and good biocompatibility (Fig. 1). The superiority of the CVA deposition method is highlighted by referencing pertinent comparative studies from the literature and by illuminating the intrinsic physics of the process, which integrates ion implantation with sputter deposition. After discussing the fundamental aspects of plasma-assisted film deposition methods, particularly the evolution and main instrumentation of the CVA technique, an overview of various characterization techniques appropriate for ascertaining the nanostructure and chemical composition of ultrathin *a*-C films is presented. Particular attention is given to the nanostructure dependence of the tribological, thermal, and mechanical properties of *a*-C films and the incorporation of a silicon-based underlayer to enhance the interfacial adhesion and elemental diffusion barrier characteristics of less than 5-nm-thick *a*-C films. The correlation of nanostructure and tribo-thermo-mechanical properties of *a*-C films is also elucidated by representative results of studies focused on the underlying physics and mechanisms of *a*-C film growth. The enhancement of the functional attributes of ultrathin *a*-C films through ultrathin underlayers is also interpreted in the context of results from recent studies. The article also provides insight into future directions and potential challenges that must be surmounted to facilitate the path towards technological innovations concerning *a*-C films.

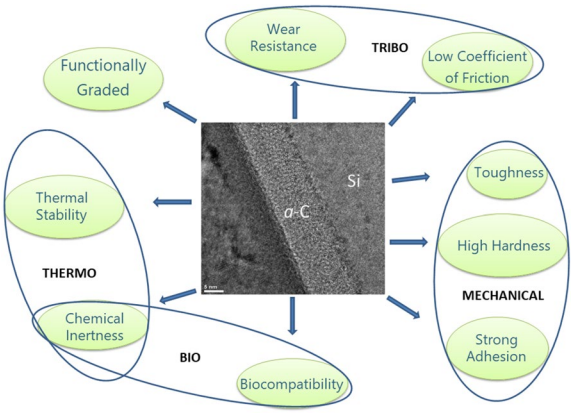

Figure 1: Illustration attesting to the excellent bio-tribo-thermo-mechanical properties exhibited by *a*-C films.

Plasma-assisted film deposition methods

Although film deposition can be accomplished by various coating methods, uniform deposition of ultrathin films necessitates a precise control of the generation and transport of the film precursors. Since plasma-assisted film deposition techniques enable the uniform growth of nanometer-thick films, they have been widely used in several leading-edge technologies, such as micro/nanoelectronics, information storage, photonics, and energy harvesting systems. An overview of the main characteristics of common plasma-assisted deposition techniques is given in this section, using results from studies dealing with the synthesis of thin and ultrathin *a*-C films to elucidate the intricacies of each deposition

method. A more topical review of recent developments in physical vapor deposition processes for thin-film deposition of different materials can be found elsewhere [129], and is distinguished from this review, which focusses primarily on CVA deposited hydrogen-free *a*-C films. To that effect, this section establishes why CVA is the principal technique of choice for ultrathin *a*-C film synthesis. Pertinently, this section provides a concise overview of the functioning of different techniques (the depositional procedures), the physics of deposition, and a comparison of the relative advantages and disadvantages vis-à-vis CVA.

Radio frequency sputtering

In rf sputtering, an inert gas (e.g., Ar) is introduced into a vacuum chamber at a controlled flow rate, where it becomes ionized by applying a high negative voltage (typically, in the range of − 1.0 to − 1.5 kV) to the system's cathode (target) consisting of the film material (e.g., pure graphite for carbon film deposition) [45]. To prevent charge accumulation, the target is biased with rf voltage. Key process parameters include the forward rf power, ion current density, target voltage, working pressure, magnitude and duty cycle of the substrate bias voltage, plasma ion density, plasma and floating potential, and system geometry [16, 130–132].

Figure 2 demonstrates the operational principle of a typical rf sputtering system. As seen in this figure, the highly energetic ions of the plasma bombarding the target material cause atoms and/or clusters of atoms to be ejected from the target surface. The critical ion kinetic energy for sputtering depends on the bias voltage applied to the cathode and the cohesive strength of the target material and affects the kinetic energy of the sputtered atoms and clusters of atoms. The collisions of the latter species with the ions and electrons in the plasma cloud during their travel across the target-substrate space generate more electrons and photons, contributing to the plasma glow. However, the low kinetic energy of the sputtered species is not conducive to film densification and sp^3 hybridization during *a*-C film growth. This shortcoming is offset by applying a negative bias voltage to the substrate, inducing ion bombardment onto the growing film. An optimum bias voltage for maximum sp^3 hybridization in *a*-C films is typically in the range of about −100 to −200 V [133]. The collision cascades between impinging Ar^+ ions and atoms at the film surface lead to atom–atom interactions at the growing film surface, resulting in film densification, intermixing of film atoms with surface atoms of the substrate [134], and the growth of diamond nanocrystallites [135], consequently producing a layered *a*-C film structure [136]. Higher voltages intensify the ion bombardment, causing film damage, thermal spikes that may trigger sp^3-to-sp^2 rehybridization, and likely resputtering of the deposited film. Substrate biasing usually leads to the incorporation of a small amount of Ar^+ ions

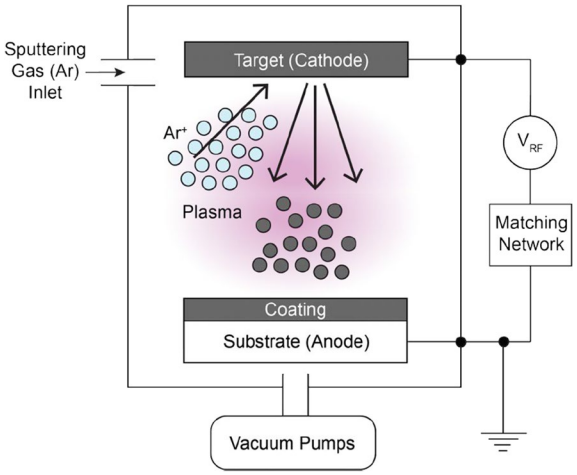

Figure 2: Schematic of the radio-frequency sputtering method [206].

(i.e., ~ 2 to 3 at%) into the film structure [19, 137]. Two major restrictions of rf sputtering are the line-of-sight deposition and the deposition of clusters of atoms, limiting three-dimensional (3D) film deposition and affecting the film uniformity, respectively.

Reactive rf sputtering is a slightly modified version of rf sputtering. In this deposition process, either a pure N_2 gas or an Ar/N_2 gas mixture is used to generate the plasma, with N^+ ion bombardment inducing film nitrogenation [45, 138, 139]. This method has been used to synthesize nitrogenated *a*-C films (*a*-CN_x) [45, 139] and to form a SiN_x underlayer by nitrogenating the Si substrate of *a*-C/SiN_x/Si stacks before depositing the *a*-C film [82]. The former technique can also be tailored to enhance the strength of the topmost atomic planes of *a*-C films (surface layer), which exhibit properties inferior to those of the underlying bulk layer, more importantly for ultrathin *a*-C films with a bulk layer thickness similar to that of the weaker surface layer.

Magnetron sputtering

Although sputtering is widely used to synthesize thin films, the deposition rate is relatively low and the plasma mainly comprises Ar^+ ions; thus, the substrate bias affects only a small fraction of the particle flux. Magnetron sputtering was originally developed as a modification to the conventional sputtering method with an objective to enhance the degree of plasma ionization and can be operated in either dc mode [140–142] or rf mode [143], similar to the conventional sputtering technique. Other variations of magnetron sputtering are high-power impulse magnetron sputtering, which successfully integrates the magnetron source with a pulsed power supply [20, 144], and ion-beam assisted magnetron, which integrates ion beam deposition with dc magnetron sputtering [145]. Reactive rf or dc magnetron sputtering that

uses either pure N_2 or N_2/Ar mixture as the sputtering gas can also be used to synthesize a-CN_x films [146–149]. As shown in Fig. 3, a fundamental characteristic of magnetron sputtering is the strong magnetic field parallel to the cathode surface generated by magnets placed right behind the target. While the sputtering process is not different from rf sputtering, magnetron sputtering uses a strong magnetic field to confine or trap the plasma electrons within the electric sheath of the target. These electrons bounce back and forth within the vicinity of the target surface until they collide with the sputtered neutrals, increasing the ionization probability of the sputtered material and, in turn, contributing to the establishment of a continuous self-sputter mode. This demonstrates the importance of secondary electron emission [20] in sustaining the process. The enhancement of the degree of plasma ionization is beneficial because the substrate bias voltage assists the implantation of the target material and the densification of the growing film, two steps that profoundly aid in the creation of hard, strong, and well-adhered films.

Similar to rf sputtering, several key process parameters, including the strength of the magnetic field, power, substrate temperature, sputtering gas composition, working pressure, and substrate bias voltage, must be adjusted to obtain the optimal deposition window for each film [141, 142, 150]. In addition, the geometrical configuration of the magnets relative to the target and the target-substrate distance influence the particle flux ratio, i.e., the relative ratio of the neutrals, ionized target atoms, and Ar^+ ions in the plasma cloud. It has been found that a-C films deposited by magnetron sputtering demonstrate good mechanical properties and adequate thermal stability, although a-C films synthesized by FCVA may exhibit even better thermal stability [151] and tribomechanical properties [140].

Ion beam sputtering

In this deposition process, a high-energy Ar^+ ion beam sputters off atoms and clusters of atoms from a target consisting of the desired film material, which subsequently deposit onto the substrate to be coated [45]. At the same time, a second Ar^+ ion beam of lower energy bombards the material that arrives at the substrate surface, assisting in film densification. The ion-beam sputtering process that utilizes a dual-ion source is depicted in Fig. 4. The ion beam energy and incidence angle strongly affect the sputtering rate of the target material and, consequently, the microstructure of the growing film. In addition, the thermal properties of the substrate material may also influence the film microstructure. For example, a high temperature and a low thermal conductivity substrate material promote the growth of graphitic carbon films, whereas cryogenic temperatures (77 K) are conducive to the growth of carbon films rich in sp^3 hybridization [152]. This can be attributed to the rapid thermal quenching of the deposited species and the fast removal of the excess energy, which prevents the development of thermal spikes that tend to destabilize the sp^3 bonding. Nonetheless, comparative studies have revealed that the quality and functionality level of ion-beam sputtered films are inferior to those of FCVA-deposited films of similar thickness [51]. The atom clusters ejected as a result of ion bombardment onto the target may degrade the uniformity and exacerbate the surface roughness of the deposited film, especially in the case of ultrathin films of thicknesses only a few nanometers. This problem cannot be overcome by means of substrate biasing, because the film precursors are primarily neutrals. The energy and incidence angle of the Ar^+ ions impinging onto the film surface must be tuned to minimize the effect of macroparticle deposition [152].

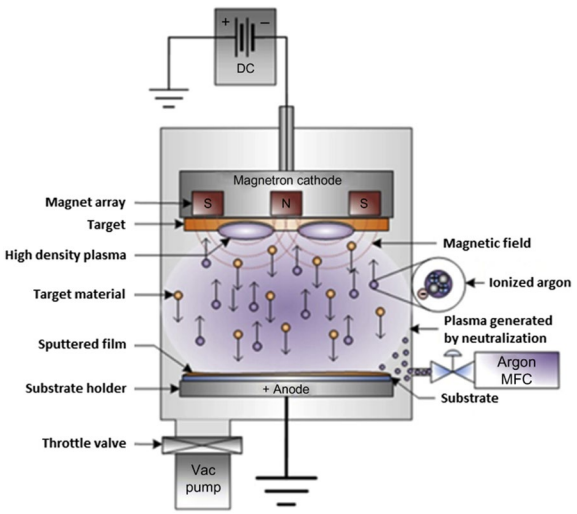

Figure 3: Schematic of the magnetron sputtering method [265].

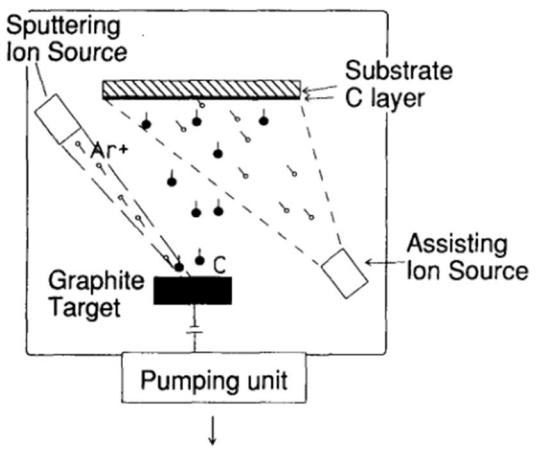

Figure 4: Schematic of the dual-source ion beam sputtering method [145].

Pulsed laser deposition and ablation

The PLD and PLA deposition methods have been used to synthesize various films, including multicomponent oxides, dielectrics, superconductors, and carbon films, because of their inherent advantages, such as the wide energy range available for particle ablation, which offsets the dependence on an external ion acceleration source (e.g., substrate biasing), room-temperature deposition, capability to tailor the process parameters to indirectly control the film microstructure (e.g., from *a*-C to nanophase diamond [153, 154]) and, in turn, the tribo-thermo-mechanical properties of the film, and, finally, the ability to grow both hydrogen-free and hydrogenated carbon films. Hydrogenated amorphous carbon (*a*-C:H) films can be grown by introducing a hydrogen buffer gas in the vicinity of the ablation site that interacts with the hot plasma plume. Hydrogen-free carbon films can be deposited either in high vacuum or in the presence of a non-reactive buffer gas like He [155, 156]. While buffer gas-carbon species interactions absorb a fraction of the translational energy of the ablated particles, this does not occur in high-vacuum deposition, consequently affecting the resulting film microstructure, particularly the formation of graphitic clusters.

Figure 5 illustrates the working of the pulsed laser deposition method. In the PLD and PLA methods, a pulsed laser beam is directed towards a target inside a vacuum chamber, and the evaporated species produced by the ablated target material condense onto the substrate surface. In the foregoing ejection process, melting of the target material due to the absorption of the photon energy of the laser beam is followed by plasma formation, the ionization and evaporation of the target material, and, lastly, the explosive ejection of target material in the form of a highly directed flux of a plasma plume [157] that contains neutrals and ionized species (i.e., singly ionized monomers, doubly ionized entities, and multiple ion charges [158, 159]) of varied kinetic energies and particulates in the form of clusters of atoms. The formation of particulates is a potential source of contamination for the deposited films because they can blemish

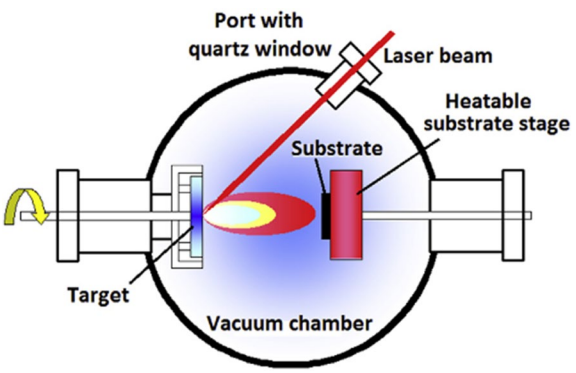

Figure 5: Schematic of the pulsed laser deposition and ablation (PLD/PLA) method [265].

the uniformity and integrity of the film. In addition to film contamination, the rapid expulsion of particulates from the target surface may accelerate the target erosion [160].

There are several key process parameters that need to be tuned in order to tailor the film microstructure and properties, including the type of the laser (typically, KrF, ArF, XeCl, or Nd:YAG excimer laser), the laser beam wavelength and fluency, the substrate bias voltage and temperature, the target-substrate distance, the pulse duration and rate of pulse repetition, the incidence angle of the laser beam, the incorporation (or not) of a buffer gas during ablation, and the rotational speed of the target. The optimum kinetic energy of the carbon species for PLD-deposited *a*-C films is ~ 90 eV [161], whereas the inherent energy of most depositing species in PLD is ~ 10 to 12 eV [162]. Important modifications of standard PLD and PLA deposition techniques include a ring electrode capacitively coupled to the target in the space between the target and the substrate [163], a rod electrode that aids the high-current discharge introduced in the same space [164], a Faraday cage integrated with an accelerating grid for the ions in the plasma plume [165], and a laser beam splitter to enable the co-deposition on a larger substrate from two targets of the same material [166]. The most important obstacles in the foregoing methods are the high initial cost of the laser system, the restricted substrate size owing to the highly oriented nature of the plasma plume, the limited target-substrate distance necessitated by the exponentially decreasing flux from the target surface, the issues surrounding film uniformity, and the generation and incorporation of particulates into the film. The latter problem may be overcome (at least partly) by using a second pulsed laser beam of low incidence angle to ablate the protruding macroparticles.

Plasma-enhanced chemical vapor deposition

The PECVD method has also been widely used to deposit thin films of various compositions. However, contrary to conventional CVD, this method uses rf discharge to decompose the film-precursor gas molecules to radicals, ion species, and electrons inside the reaction chamber. The dissociation and activation of the precursor gas culminates in plasma formation through the rf discharge process, offsetting the high substrate temperatures needed in CVD reactors to initiate reactions at the substrate surface via excessive heating. Hence, the plasma acts as an activation source rather than a high temperature, eliminating the need for a high-temperature reactor. Electron cyclotron resonance chemical vapor deposition [3, 167, 168] is a new variant of PECVD that has been gaining traction lately; however, the discussion herein is restricted to standard PECVD.

Figure 6 shows the general working principle behind the PECVD process. In the rf PECVD process, the substrate is placed on a platen inside the reaction chamber, which is heated

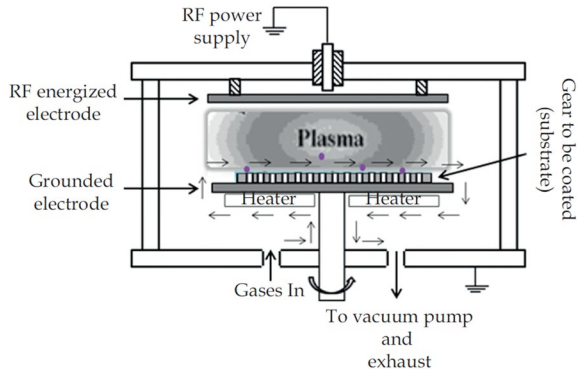

Figure 6: Schematic of the plasma-enhanced chemical vapor deposition (PECVD) method [266].

until the desired deposition temperature is reached at the substrate surface. The system is then pumped down to remove any adsorbents from the chamber walls before introducing the precursor gas in the chamber. Among various precursor hydrocarbon (C_xH_y) gases used to synthesize *a*-C:H films, the most commonly used are acetylene [110, 140, 169–172], methane [173–176], ethylene [112, 177], and benzene [175]. To enhance the dissociation of the hydrocarbon gas, a diluting carrier gas (e.g., hydrogen) may be incorporated in the gas mixture; however, hydrogen dilution can affect the hydrogen content of the film. A precise control of the pressure in the reaction chamber (typically in the range of 10–100 mTorr [112, 140, 170–173, 176]) is necessary for sustaining the plasma. The rf power applied between the electrodes ionizes the gas mixture in the reaction chamber, and the produced chemically reactive species (e.g., $C_xH_y^+$ for hydrocarbon precursor gases) dissociate at the substrate surface forming a film [45]. To improve the film quality, an Ar gas may be introduced into the reaction chamber [171, 172, 174] to induce Ar^+ ion bombardment onto the growing film, etching away the softer species and aiding in film densification. A negative bias voltage between −50 and −300 V [140, 169–171, 173] can also be applied to the substrate by an external dc power supply to augment the aforementioned densification process. Furthermore, adding nitrogen gas in the precursor gas mixture is an effective method for synthesizing nitrogenated films, such as *a*-CN:H [174, 177].

Because the hydrogen incorporated into the film microstructure is detrimental to the mechanical properties, it is beneficial to use a precursor hydrocarbon with a low hydrogen-to-carbon ratio (e.g., acetylene) to reduce the hydrogen content of the film. Additionally, precursors of low ionization potential, such as benzene, can be used to increase the growth rate. Thus, the choice of the precursors and secondary gases (i.e., H_2 or Ar) has a profound effect on the properties of *a*-C:H films [45]. Studies have been carried out to identify the role of key process parameters, such as frequency of discharge [175], substrate bias voltage [171], rf power [176], and substrate temperature [169, 170]. For instance, the highest density and hardness of *a*-C:H films grown by PECVD were found for a 50 W rf power [176]. Several PECVD studies have been performed at temperatures between room temperature [170, 173, 174, 176] and 250 °C [112, 140, 169, 170]. Although an elevated substrate temperature activates the reaction species and yields more products, it may also degrade the film quality. In the case of carbon films, for example, a high substrate temperature during deposition may induce graphitization and film delamination upon cooling. Thus, an optimum temperature window must be identified for each film deposited by PECVD. In addition to the rf power and substrate temperature, the gas flow ratio (C_xH_y:H_2:Ar:N_2) also plays an important role, because it affects the composition, hydrogen concentration, and final microstructure of the *a*-C:H films.

Thin films formed by PECVD are predicated on the adsorption of precursor species onto the substrate surface via chemisorption, i.e., the process does not produce implantation and/or intermixing with the substrate material as in other energetic condensation techniques. This can culminate in problems pertaining to adhesion with the underlying substrate. Concerning PECVD-synthesized *a*-C:H films, while a high self-bias voltage yields good-quality films, a low self-bias voltage produces polymer-like film microstructures containing up to 70% hydrogen and consisting of long hydrocarbon chains [110, 171] rather than diamond-like microstructures. In addition, PECVD cannot be used to synthesize hydrogen-free films. The presence of hydrogen in the carbon film microstructure not only impacts the mechanical properties but also affects the thermal stability. For instance, studies of the thermal performance of PECVD-deposited *a*-C:H films and FCVA-deposited *a*-C films revealed an inferior thermal stability of the *a*-C:H films at elevated temperatures because the effusion of hydrogen weakened the film microstructure and resulted in morphological changes, e.g., film surface roughening [110, 112]. Similar findings were obtained from an investigation in which carbon overcoats prepared by PECVD failed through extensive graphitization and oxidation at elevated temperatures [177]. In another comparative study [140], PECVD-based *a*-C:H films were found to be inferior to *a*-C films deposited by FCVA, direct ion-beam deposition, or magnetron sputtering, in terms of their overall mechanical performance, i.e., scratch and wear resistance, propensity to produce wear debris, and adhesion to the substrate.

Plasma-based immersion ion implantation and deposition

The PIIID method was developed in the 1980s [178, 179] and is considered as the predecessor of the FCVA technique. The PIIID was initially used as a surface modification process to case harden cutting tools (mostly steel-based tools) by nitrogen implantation

and was later extended to encompass virtually all solid metals in the periodic table [180, 181] and carbon. This surface treatment method can be used to protect surfaces in numerous applications, including biomedical instruments [182], magnetic recording heads [183], and various metallic, plastic, and ceramic substrates. The PIIID is also known as plasma-source ion implantation, plasma-based ion implantation, plasma immersion ion implantation, plasma-based ion implantation and deposition, and metal plasma immersion ion implantation and deposition; nevertheless, the fundamental process is essentially the same. The PIIID process has been integrated with a wide variety of plasma-producing techniques, such as inductive rf plasma of Ar and C_2H_2 [184, 185], CVA [183, 186–192], and rf glow discharge plasma [193]. The latter methods are used to assist in the generation of the plasma, with the PIIID proceeding thereafter with the actual film formation on the substrate surface.

In conventional ion implantation, the ions extracted from a plasma source are first accelerated to achieve the desired kinetic energy and then uniformly deposited onto the target substrate. However, this method possesses certain inherent limitations [178], such as the line-of-sight restriction, which prevents plasma purification, the accommodation of a relatively small target that must be continuously rotated to ensure uniform treatment of all sides, the usage of extra heat sinks to limit the temperature rise during implantation, and the masking of the target to minimize the ion incidence angle, with the risk of film contamination due to mask sputtering. Accordingly, the original incentive for developing the PIIID process was to circumvent the above inherent limitations pertaining to conventional ion implantation. The PIIID method was conceptualized and implemented for a conductive substrate (target) directly immersed in a plasma cloud of ions of the coating material [178, 179], as schematically exhibited in Fig. 7. A thick electric sheath that surrounds the immersed target is produced by repetitive pulsed biasing the substrate to a negative voltage of the order of several kV, aiding in the acceleration of the plasma ions bombarding the substrate from all sides, uniform surface treatment, successful elimination of the problems associated with shadowing and target manipulation witnessed in conventional ion implantation, higher throughput, and reduced operation cost [179].

An inherent feature of PIIID is the negative pulsed bias voltage repeatedly applied to the substrate, which enables different surface modification processes to occur due to alternating between implantation and deposition when the negative bias voltage is on and off, respectively. When a zero or low (e.g., < 10 V) bias voltage is applied to the substrate, the low kinetic energy of the impinging ions favors film deposition onto the substrate surface. Alternatively, when a high negative bias voltage (on the order of several kV) is applied to the substrate, the growing film is intensively bombarded by the highly energetic ions, with ion bombardment inducing both direct and recoil implantation. The

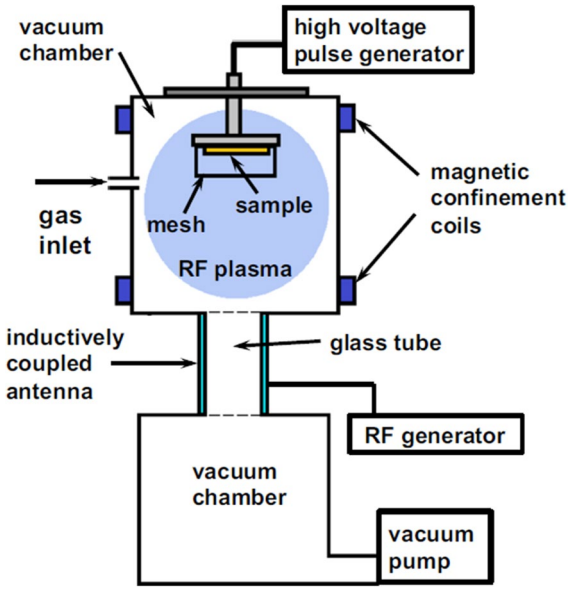

Figure 7: Schematic of the plasma immersion ion implantation and deposition (PIIID) method [267].

repeated pulsed biasing of the substrate leads to the formation of an intermixing layer, yielding a film atomically bonded to the substrate [194]. The intermixing layer enhances the adhesion between the film and the substrate, which is critical to the film's functionality and longevity. More importantly, the PIIID process allows the film microstructure to be tailored by tuning the duty cycle of the substrate bias voltage, which controls the respective durations of ion implantation and deposition in each pulse. Furthermore, unlike ion-beam assisted deposition and ion plating, which require a second ion source (e.g., Ar^+) to produce energetic species for film densification, PIIID effectively integrates this vital densification step into its implantation phase.

The PIIID is widely regarded as the predecessor of the CVA method. Nonetheless, there are several fundamental differences between PIIID and CVA. Specifically, the PIIID is inherently well-suited for 3D deposition, whereas the CVA has a certain amount of directionality associated with the plasma throughput. Thus, an advantage of PIIID compared to CVA is that a target manipulation fixture is not needed. Because the CVA is restricted to planar surfaces for uniform deposition, any form of 3D deposition would necessitate a specialized and expensive target manipulator/fixture to be integrated into the CVA setup. In addition, there are differences in the basic physical processes. For instance, in PIIID the substrate is completely immersed into the plasma cloud, whereas in CVA the substrate is placed in the path of high-purity singly charged ions which constitute the plasma. Furthermore, the PIIID is not restricted to plasma generation solely by cathodic vacuum arcing as the CVA method because the plasma can be generated by a high ac or dc voltage or even a heated filament. Alternatively, plasma ignition in CVA relies on arcing at the cathode surface initiated by

a mechanical striker or a triggerless method. The issues pertaining to the stability of plasma arcing in CVA have propelled the use of a special configuration of the anode–cathode magnetic field, the so-called 'cusp' configuration [14, 54]. This special configuration cannot be achieved if the substrate is placed very close to the cathode so that it is immersed in the plasma as in the case of PIIID. A major advantage of CVA over PIIID is the offered ability to manipulate the plasma by the magnetic fields of the solenoids surrounding the ducts. This allows for much better control over the ion flux profile that reaches the substrate. In addition, given the high negative bias voltages (about − 2.4 kV [186]) applied in the PIIID, the impinging ions penetrate much deeper (μm and sub-μm) in comparison to FCVA (nm to sub-nm), where the negative bias voltage is of the order of − 100 V [15, 113, 195]. However, ion kinetic energies above a few hundred eV can have deleterious effects on the overall integrity of the growing film, particularly in the ultrathin film regime (i.e., < 5-nm-thick films) because the extremely intense ion bombardment can cause resputtering and damage to the film. Accordingly, in applications requiring precise surface modification with minimal damage and/or alteration to the underlying substrate surface, such as in magnetic recording, optical lenses, and photonics, the CVA technique is the preferred choice of deposition. To add to this list of differences, while the PIIID allows for the formation of compound films by the addition of a reactive gas in the vicinity of the substrate during processing, it does not allow for co-deposition as in CVA, which uses separate plasma guns converging onto the substrate surface. Therefore, in the larger scheme of things, the CVA is a better nanoscale film deposition method because it provides better control over the ion flux profile reaching the substrate, enables growth of nanometer-thick films, and induces minimal surface damage and compositional changes to the substrate.

Cathodic vacuum arc

Among all the aforementioned deposition techniques, the filtered version of the CVA process (i.e., FCVA) is the most efficient method for synthesizing coherent thin and ultrathin films [1] with desirable morphological attributes [100] (e.g., smoothness) and good tribo-thermo-mechanical properties [14, 17, 54, 81, 113]. This has been established in previous comparative studies of FCVA-deposited films and films deposited by rf, ion-assisted, and magnetron sputtering [51, 100, 140, 151], PECVD [110, 112, 140], ion-beam sputtering [51], and direct ion beam deposition [140] in terms of a wide range of parameters, such as density, hardness, wear and scratch resistance, sp^3 content, and thermal stability.

The general characteristics and operational principles of the FCVA method are discussed in more depth in the following sections of this article. Further analysis of the physics of cathodic arc plasma generation has been covered in a previous article [196]. Nonetheless, the basic concept remains that FCVA is a low-voltage, high-current plasma discharge technique occurring between two electrodes placed in vacuum. Once a high voltage is applied to the cathode and arcing is initiated by a mechanical or electromechanical trigger, a trigger pulse generator, or a triggerless method, the current is sustained through the seamless generation of arcing spots through an explosive emission phenomenon at the cathode surface, which is intrinsic to this technique. Surface irregularities, such as edges and perturbations, initiate and anchor the arcing spots in their vicinities [1]. Due to the foregoing explosive arcing process, globules in the form of microdroplets (commonly referred to as macroparticles due to their enormous size when juxtaposed against ions) are ejected from the cathode surface. For film uniformity, these macroparticles must be filtered out before they reach the substrate surface. Thus, a variety of filters and duct designs have been developed [54, 64–80] to effectively remove any macroparticles that might be ejected from the cathode surface. A series of magnetic coils (solenoids) wound around the duct cause the electrons in the plasma to spiral along the duct axis due to the Lorentz force principle. This spiral motion of the electrons generates an electrostatic field that imparts certain directionality to the plasma ions. As a result, the ions follow the electrons in the plasma through the duct, guided from the cathode to the substrate on a pre-defined trajectory by a phenomenon known as ambipolar transport [45]. Non-planar ducts are particularly effective in trapping the neutral macroparticles as they travel in straight trajectories. This type of a filtering system ensures that only high purity ions reach the substrate surface, which is critical for the growth of particle-free, ultrathin films [53, 81, 82]. A schematic representing a state-of-the-art FCVA system for synthesizing ultrathin films is displayed in Fig. 8.

The intrinsic advantage offered by the FCVA method is the integration of low-energy deposition with high-energy

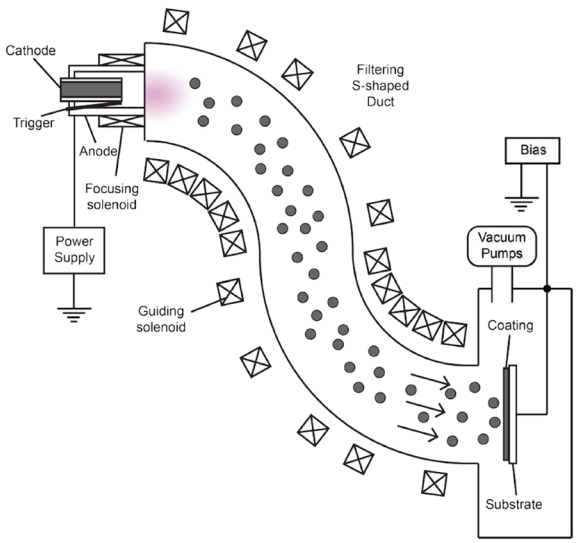

Figure 8: Schematic of the filtered cathodic vacuum arc (FCVA) method [206].

implantation process steps and the ability to control the respective ratio of both steps through the duty cycle of pulsed substrate biasing. The energetic ion bombardment onto the growing film surface encountered during the implantation phase of a duty cycle enables the removal (resputtering) of loosely bonded surface atoms, film densification, and intermixing at the film/substrate interface, which enhances the adhesion of the film to the substrate. Additionally, the intense ion bombardment during substrate biasing promotes the development of a compressive mechanical environment, which is conducive to sp^3 hybridization, resulting in the formation of diamond nanocrystallites in an otherwise graphitic matrix [197]. Considering all of the above relative advantages exhibited by the FCVA method, it may be inferred that, amongst all of the film deposition methods discussed in this section, the FCVA appears to be the most effective method for depositing thin and (especially) ultrathin *a*-C films.

General characteristics of cathodic vacuum arc systems

In CVA systems, the plasma comprises a very high degree of ionized particles, such as single charged C^+ ions, a very small fraction of doubly charged C^{++} ions, and carbon neutrals in the case of carbon plasma generated from a pure graphite cathode [198]. However, the explosive arcing at cathode spots also generates macroparticles, which inhibit the growth of dense, smooth, defect-free, uniform films. The direct (line-of-sight) deposition performed in the nascent developmental stages of this technique only exacerbated the acuteness of this problem. Macroparticle formation in the form of micrometer-size droplets or solid particulates is due to shock-heated gas inclusions at the cathode surface [70].

One of the primitive methods for preventing macroparticles from reaching the substrate surface is the use of a curved duct. The effectiveness of a curvilinear plasma-optics system to remove the macroparticles from the plasma stream demonstrated in early studies [68, 199] motivated design innovations, which further enhanced the filtering capability of CVA systems, allowing only the ions of the cathode material to reach the substrate, and, consequently, the film quality to be significantly improved. This was accomplished by winding the curvilinear duct with solenoids. As stated earlier, the high-purity, singly-charged ions are guided from the cathode to the substrate due to the ambipolar transport phenomenon [45]. Because the macroparticles have much larger masses and are not charged, they tend to travel in straight trajectories, thus becoming segregated from the high-purity ions in the plasma. Experiments with curved and straight post-arc-discharge solenoids have shown a superior macroparticle filtering efficacy of a curved solenoid system [65]. Using an annular cathode as the plasma source in CVA integrated with a straight duct has also been explored [200] but with limited success in precluding direct line-of-sight. Another design improvement is the use of ribbed ducts rather than smooth ducts, for more effective trapping of the macroparticles bouncing off the duct walls [66]. Additionally, toroid magnetic filters are more effective in producing macroparticle-free thin films. A further improvement is a rotating carousel in the coating chamber that facilitates rapid film deposition on various substrates [67]. However, in the CVA designs comprising a 90° bend duct with winded solenoid coils, the magnetic field lines intersect the duct walls at the entry and the exit locations. To surmount this problem, certain design modifications have been considered [69], such as the addition of extra current-carrying solenoid coils strategically located not only along the filter but also at the entrance and the exit of the filtering duct. This design modification results in more plasma from the source to be injected into the filter and also reduces the divergence of the magnetic field lines, thereby enhancing both the efficiency and throughput of the deposition process. Besides the aforementioned design changes, applying a positive bias voltage of ~ 20 V to the duct can increase the filtering efficacy [201, 202].

Advances in microdevice technologies that rely on ultrathin films to protect vital components prompted additional developments in the filtering capabilities of CVA systems. Particularly, improvements in duct instrumentation further enhanced the particle filtration efficiency, which was dictated by growing demands for high-quality films of thickness only a few nanometers. Hence, several innovative duct-filter designs were introduced to augment the level of particle filtration, such as 45° filters [71] also known as knee filters, 45° double-bend filters [79, 117], filters with different rectangular cross sections [74, 75], segmented filters [73, 78], single 90° bend filters [126, 201, 203], in-plane S-shaped filters [72], twist filters [204], and second-generation planar filters with two 90° bends twisted by 45° [70]. However, despite these new filtering designs, particle reflection from the duct walls persisted even with ribbed duct structures, leading to the growth of films with embedded particles. While using an open filter [65, 70] circumvented the problem of multiple particle reflections from the duct walls, it prevented low-pressure film deposition because it allowed ambient gaseous species to enter the duct unhindered. A significant breakthrough in filtering systems was the introduction of the out-of-plane double bend [76, 77] and the out-of-plane S-configuration closed filter [54, 64]. The latter filtering system enables the deposition of particle-free films as thin as 1–4 nm [53, 82]. Further developments with the foregoing filtering system led to the design of a cusp-configuration magnetic field in the vicinity of the anode that stabilized plasma arcing at the cathode surface by maintaining the arc current [14, 54], ensuring an uninterrupted electron flow from the cathode to the anode.

A high to ultra-high vacuum typically between ~ 10^{-6} and ~ 10^{-8} Torr [53, 70, 81, 82, 100, 121, 122, 124, 126, 205, 206] is maintained throughout the deposition process to remove any gases adsorbed onto the chamber walls and other contaminants present therein. In the case of a high-purity graphite cathode, this ensures that only C^+

ions are deposited onto the substrate, the overarching goal being the synthesis of high-quality *a*-C films. Plasma arcing in CVA systems is commonly induced by either a mechanical trigger that strikes the high-purity cathode (99.99%) to ignite the plasma [14, 53, 54, 81, 82, 98, 205, 207], or an arc initiation process [56–61, 208–210] involving the application of a low arc voltage, provided a conducting path exists between the electrodes. The latter can be achieved by separating the anode from the cathode by an insulating material (e.g., ceramic) and coating the cathode and insulator surfaces with a conductive metallic or graphitic layer, depending on the cathode material. To prevent the contamination of the deposited film, the cathode material is often used as the conductive coating. Upon applying the arc voltage, plasma ignition causes an explosive destruction at the cathode-coating interface due to localized Joule heating, consequently eliminating the need for a mechanical trigger or a trigger pulse generator [208–210]. The erosion of the insulating coating is minimized by ensuring that the coated insulator and the cathode spots are not in the line of sight. While this process reduces the deposition rate of the cathode material, it averts film contaminants [209].

Although the foregoing discussion is restricted to single-cathode CVA systems, innovations in dual-cathode/dual-source deposition designs [56–63] have also been motivated by demands for hybrid films exhibiting enhanced functionalities, particularly *a*-C:M (M = Ti, W, Mo, Cr, Nb, Pd, or Pt) films. Figure 9 shows schematically the foregoing key designs of dual-cathode/dual-source FCVA co-deposition, i.e., a system with two plasmas originating from two different cathodes, which use the same duct space to reach the substrate [Fig. 9(a)], and a system with two separate plasma streams, which use two different ducts to deposit a film on the same substrate [Fig. 9(b)]. These dual-cathode designs were inspired by CVA systems that use two miniature plasma sources to deposit *a*-C:W films [62]. In addition to the co-deposition of two different materials, such as *a*-C and metal from high-purity graphite and metal targets, respectively, the dual-cathode CVA systems provide the advantage of tailoring the microstructure of the hybrid film by species selective biasing [57, 59–61] and by controlling the carbon/metal deposition pulse ratio, which determines the respective fluxes of the two constituent elements in the film [57]. In most systems, pulsed biasing is applied only to the carbon cathode and is turned off during the deposition of the metal. This is accomplished by a computer-controlled bias amplifier that synchronizes the substrate bias with the pulsed mode generation of different plasmas. [59] The reason for applying species selective biasing is that the charge state of the metal ions produced from the cathode by plasma arcing is typically equal to + 2 or + 3 and their energy is ~ 50 eV [60]. If a uniform bias voltage is applied to both the carbon and the metal cathodes, the kinetic energy of the heavier and more charged metal ions impinging onto the substrate surface will be much higher than that of the C^+ ions, resulting in excessive resputtering of the deposited film

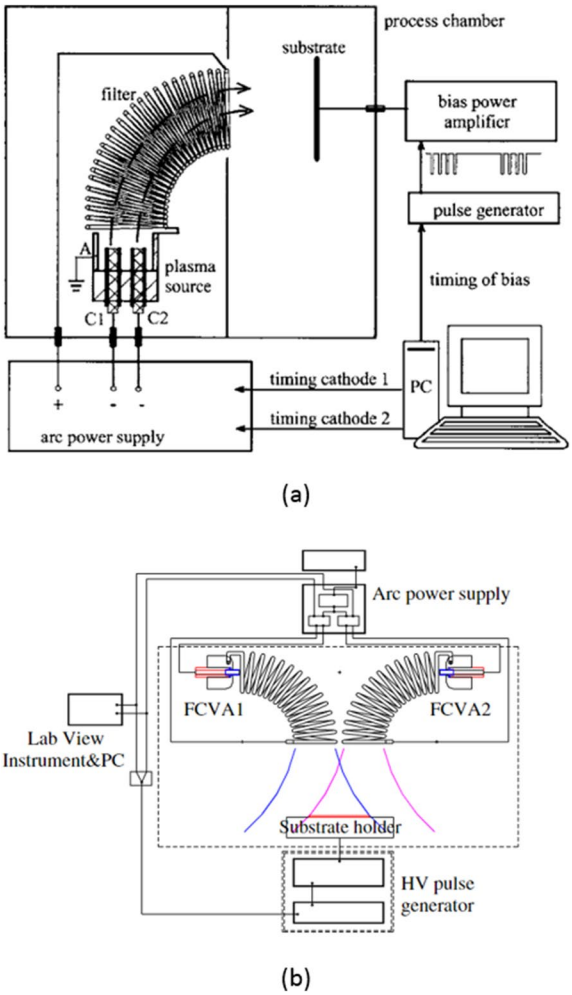

Figure 9: Schematics of two different designs of dual-cathode/dual-source FCVA deposition with selective pulsed biasing allowing for co-deposition to form *a*-C:M thin films: (a) a system that uses the same duct space with two different cathodes producing two different plasma streams [60], and (b) a system with two separate plasma streams coming from different ducts and converging on the substrate surface [56].

and the development of thermal spikes that may compromise sp^3 hybridization and, in turn, the functional attributes of the film. Therefore, it is essential to control the kinetic energy of the charged particles arriving at the substrate surface via selective tuning of the bias voltage.

Another advantage of the CVA method that enables the deposition of high-quality films is the regulation of the kinetic energy of impinging ions through the modulation of the substrate bias voltage. Usually, there is an optimum substrate bias voltage for attaining films with excellent tribo-thermo-mechanical properties [10, 15, 17, 103, 113, 195, 211]. A relatively high substrate bias voltage (e.g., − 400 V) intensifies the ion bombardment onto the growing film surface, inducing resputtering and damage. Alternatively, a relatively low substrate bias voltage (e.g., − 20 V) favors deposition but is counter conducive to direct and

recoil implantation, which are responsible for film densification, the development of a highly compressive stress environment that is critical for sp^3 hybridization, the preferential removal of weakly bonded atoms, and the formation of an intermixing layer that enhances the bond strength of the film to the substrate. A thicker intermixing layer not only increases the interfacial bond strength but may also reduce the large stress/strain gradients at the film/substrate interface, thereby providing a gradual transition between the structure and properties of the metallic substrate and the *a*-C film. However, in certain applications, a relatively thick intermixing layer may be detrimental to the material properties. For example, a thick intermixing layer may alter or even corrupt the magnetic properties of the underlying magnetic medium of hard disks, or its elements may diffuse deeper into the substrate compared to a thin intermixing layer in elevated-temperature applications, such as HAMR disk drives and laser photonics. Therefore, the optimum range of the intermixing layer thickness also depends on the operation conditions of the device.

The CVA method may be thought as an integration of conventional sputtering deposition and plasma-assisted implantation techniques. In the absence of a substrate bias voltage, a deposition process that resembles sputtering occurs (although the film precursors are charged particles in CVA rather than atoms and/or clusters of atoms as in sputtering) because the low kinetic energy (typically, 20–25 eV, depending on the plasma type [39, 115]) of the target ions favors the dominance of the deposition process. Alternatively, when a bias voltage is applied to the substrate, the increase of the kinetic energy of the charged particles favors direct and recoil implantation in conjunction with sputtering of the weakly bonded atoms. Although sputtering tends to reduce the film thickness, direct/recoil implantation and sputtering enhance film densification. The relative contributions of deposition versus direct/recoil implantation and sputtering can be controlled by tuning the duty cycle of the pulsed bias voltage applied to the substrate. For example, a duty cycle of substrate pulsed biasing of 80% (i.e., on and off substrate biasing for 80% and 20% of the pulse period, respectively) results in dominant direct/recoil implantation and sputtering for 80% of the pulse period and dominant deposition for 20% of the pulse period. Usually, the optimum duty cycle of substrate pulse biasing is 65% for 10–20-nm-thick *a*-C films [52] and 50% for 70–100-nm-thick *a*-C films [186]. An advantage of CVA deposition is that there is no line-of-sight issue as with most other deposition techniques because the energetic ions (film precursors) accelerate through the thin electric shield that surrounds the substrate. Accordingly, the capability to control the energy and trajectory of the film precursors allows for versatile deposition, which is especially beneficial for coating components with complex geometries. Characteristic features and design intricacies of different CVA systems are summarized in Table 1.

TABLE 1: Characteristic features and design intricacies in different CVA systems.

Design component	Type	Magnitude/sub-type	References
Macroparticle filter/duct design	Primitive designs exploring initial curvilinear plasma physics		[68, 199]
	Annular cathode integrated with a straight duct		[200]
	Direct line-of-sight deposition with no macroparticle filter		[65]
	Duct walls	Ribbed duct	[66]
		No walls (open filter)	[65, 70]
	Bent filters (angle of bend)	45°	[71, 79, 117]
		90°	[17, 69, 126, 140, 201, 203]
	Rectangular cross-sectioned duct		[74, 75]
	In-plane S-shape configuration		[72]
	Out-of-plane configuration	S-shaped	[54, 64]
		Double bend	[76, 77]
		Twist filter	[204]
CVA systems	Single cathode		[14, 41, 52–54, 64, 81, 82, 97, 98, 100, 110, 112, 232, 256]
	Dual cathode or dual source arrangements for co-depositing *a*-C:M films		[56–63]
Initiation of plasma arcing	Mechanical striker (mechanical triggering)		[14, 17, 53, 54, 81, 82, 98, 205, 207]
	Trigger less initiation of plasma arcing		[56–61, 208–210]
Magnetic field stabilization	Direct line-of-sight deposition without magnetic coils		[65]
	Curved solenoid coil		[65]
	Strategically located solenoid coils at entrance and exit		[69]
	Cusp configuration magnetic field near the cathode for stabilizing the arc current		[14, 53, 54, 81, 82]

Microanalysis methods

Synthesis of ultrathin films using plasma-assisted techniques, such as the CVA method, is of paramount importance. However, in conjunction with film synthesis, there is also a growing challenge with regards to characterizing these films as their thickness is reduced due to recent technology demands. Characterization comprises nanoscale imaging to determine the thickness, ascertaining the nanostructure and composition, and assessing the tribomechanical characteristics of thin films.

Among various microanalysis techniques, X-ray reflectivity (XRR) has been commonly used to analyze monolithic and layered thin films utilized in various technologies (e.g., optoelectronics), particularly for estimating the film density. This technique uses a critical angle, which in essence is the grazing angle of an X-ray of a certain wavelength, to calculate the mass density. Several XRR studies have been devoted to the effects of heat treatment and thermal annealing on the density and composition of *a*-C films [91, 212–215]. A very good agreement in film thickness and surface roughness values was obtained by combining XRR with AFM, TEM, and spectroscopic ellipsometry [215]. An XRR analysis of ultrathin (2–5 nm) *a*-C films has shown that, for such small thickness, the X-rays penetrated the films and were reflected back by the silicon substrate [216].

X-ray photoelectron spectroscopy (XPS) is another microanalysis method widely used to characterize the structure and composition of various films. Specifically, the sp^2 and sp^3 fractions of *a*-C films can be obtained from the deconvolution of the C 1*s* core-level peak of the XPS spectrum [14, 96]. Changes in the nitrogen pressure and substrate bias during the growth of nitrogenated amorphous carbon (*a*-C:N) films have been reported to correlate with the shift of the N 1*s* peak in the XPS spectrum [217]. Also, the deconvoluted C 1*s* and N 1*s* peaks of the XPS spectrum of *a*-C and *a*-C:N films have been used to analyze the near-surface chemical composition and to compute the sp^3/sp^2 ratio [218–223]. Important insight into changes in the film composition can be obtained by studying the major shifts of the C 1*s* and N 1*s* peaks.

X-ray diffraction (XRD) at small grazing angles can be used to analyze the microstructure of thin-film materials. For example, structural characterization by XRD has revealed nanocrystallites of diamond [83] and metal nanoclusters in *a*-C:M (M = Au, Ag, Cu, Mo, or Ti) films above a certain threshold of metal concentration, e.g., 14.8 at% Cu for *a*-C:Cu films and 1.5 at% Ag for *a*-C:Ag films [61]. Although XRD was not effective in detecting the existence of crystalline phases in low (1.2–12.5 at%) Ti content *a*-C:Ti films, a TiC crystalline phase was found in *a*-C:Ti films with a relatively high (21.4–46.0 at%) Ti content [86]. Similar findings were reported in another XRD study of *a*-C:Ti films where the formation of crystalline TiC was only observed for Ti contents of 10–20 at% [84]. In addition to structural analysis, XRD was used in the foregoing investigation to measure the residual stress in the films. In another XRD study of FCVA-deposited *a*-C films, post-deposition Ar^+ ion irradiation was found to change the broad XRD reflections in the diffractogram of the as-grown films (indicating the formation of an amorphous phase) to well-defined reflections revealing the growth of nanocrystals in the irradiated film [85].

Raman spectroscopy is an effective method for characterizing the composition, stress/strain state, and crystal symmetry and orientation in *a*-C films. For visible excitation, the Raman spectrum of carbon films typically contains two characteristic peaks, known as the D and G peaks, which are centered at approximately 1360 and 1560 cm^{-1}, respectively [224]. Because visible excitation resonates with π states, the Raman spectra are dominated by the sp^2 sites; therefore, both G and D peaks are due to the sp^2 sites. The G peak is associated with bond stretching of all pairs of sp^2 atoms in both rings and chains, whereas the D peak is linked to the disorder of activated breathing modes of sp^2 atoms in the hexagonal rings of the graphitic structure. The upward shift of the G-peak position, the dispersion of the G peak, and a low or zero I_D/I_G ratio may be interpreted as an increase of the sp^3 content of the film [225, 226]. Consequently, the absence of the D peak may be viewed as an indicator of a high sp^3 fraction [94, 227]. Moreover, the I_D/I_G ratio and the linewidth of the G peak can be used to estimate the size of the aromatic clusters and approximately the sp^3 fraction in carbon films. This becomes more relevant when studying processes that alter the carbon film composition, such as thermal annealing. For instance, a Raman analysis showed different variations of the I_D/I_G ratio of thermally treated *a*-C films prepared by CVD and FCVA, revealing better thermal stability for FCVA-deposited *a*-C films [112]. In other studies, Raman spectroscopy was used to correlate the microstructure characteristics (e.g., atomic hybridization) of *a*-C films with the tribomechanical properties [228], or to track changes in the shape, peak position, line width, and relative intensities of the D and G peaks due to the variation of the input parameters, such as the substrate bias voltage [217] and the deposition temperature [222].

Despite valuable insight gained from the foregoing microanalysis techniques, characterization of ultrathin films (i.e., < 5 nm thick) by these methods is ineffective due to physical limitations. In particular, XRR cannot accurately measure the density of films with thickness less than ~ 20 nm, XPS uses the chemical shift between sp^2 and sp^3 hybridizations in the C1s spectrum to assess the overall composition up to a depth of ~ 10 nm, Raman is only sensitive to sp^2 hybridization and is typically used to indirectly interpret the sp^3/sp^2 ratio by the first-order D-to-G band ratio, which lacks accuracy, especially when applied to ultrathin films, and, more importantly, none of the former methods can yield through-thickness depth profiles of the structure of ultrathin films [81, 82].

The intrinsic high resolution of TEM makes it particularly effective in characterizing the structure of ultrathin films [115, 229]. For example, TEM characterization has shown the formation of diamond nanocrystallites in FCVA *a*-C films [197] and the growth of diamond-like carbon (DLC) films with bulk layers of uniform density for carbon ion energy between 60 and 160 eV [44]. The TEM was also used to reveal the layered structure of thin *a*-C films synthesized by PLD [101] and FCVA [41]. High-resolution TEM was used to image the microstructure of ~ 100-nm-thick *a*-C films grown by FCVA and annealed in the temperature range of 150–600 °C for possible vertically oriented carbon sheet applications [230]. A distinct 3-nm-thick intermixing layer consisting of C, Si, and possibly SiC was observed in TEM images of cross-sectional samples of 55-nm-thick *a*-C films deposited on Si substrates by FCVA [44], which was attributed to the subplantation process [231]. A typical TEM micrograph revealing the different layers in a Si/SiN_x/*a*-C/Cr stack is shown in Fig. 10(a).

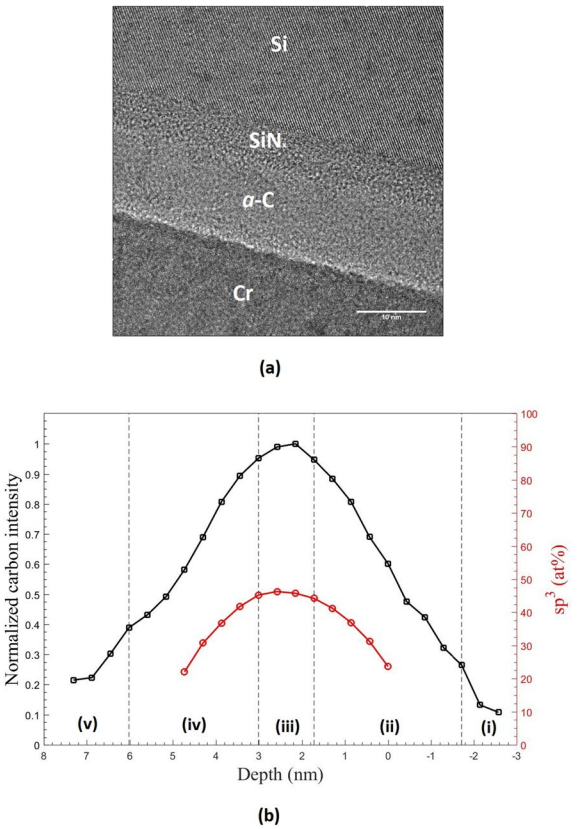

Figure 10: (a) Typical TEM micrograph revealing the layers of a Si/SiN_x/*a*-C/Cr stack. (b) Depth profiles of normalized carbon intensity (black curve) and sp^3 atomic carbon hybridization (red curve) calculated from the C K-edge EELS spectrum of an *a*-C film in a Si/*a*-C/Cr stack. The EELS depth profiles evince a layered cross-sectional structure consisting of (i) Si substrate, (ii) intermixing layer, (iii) bulk layer, (iv) surface layer, and (v) Cr capping layer. This figure illustrates how the integration of TEM with EELS can comprehensively characterize ultrathin *a*-C films by providing both imaging and nanostructure data.

While the TEM is an effective method for inspecting a film's uniformity, continuity, and conformity to the substrate surface, it also has its own limitations. For example, the TEM cannot reveal local changes in the structure/composition based on structure (crystalline or amorphous) and visual contrast differences, and, more notably, it fails to accurately distinguish the boundaries of different layers, such as the intermixing, bulk, and surface layers comprising the structure of *a*-C films synthesized by energetic particles, as the C^+ ions in the FCVA method. Moreover, the TEM cannot identify individual atoms and microstructural entities that may diffuse across different layers of a stacked configuration. This is more so at elevated temperatures similar to those of HAMR drives and laser photonics, where the thermal energy absorbed by the carbon atoms enables them to overcome the energetic barrier to diffusion, leading to interlayer elemental diffusion that cannot be distinguished by the TEM.

The former limitation can be overcome by combining TEM with EELS to enable the identification of an element based on its actual chemical fingerprint. In particular, the EELS method can be used to measure the sp^2 and sp^3 contents of vacuum-deposited DLC films [104, 105] and to study the effect of the substrate bias voltage on the hybridization state of FCVA-deposited *a*-C films [90]. By integrating the TEM with the EELS, a very small step size (~ 0.2 nm) and a sub-nanometer sampled area can be achieved, which are essential for cross-sectional analysis of ultrathin films. These intrinsic features of this hybrid technique facilitate the normalized carbon intensity and hybridization depth profiles to be obtained from the C K-edge EELS spectrum of carbon films as thin as 1–3 nm [41, 52, 53, 98, 100, 232]. The discovery of the layered structure of *a*-C films synthesized by energetic particles, consisting of an intermixing layer with greatly varying sp^3 fraction, a bulk layer with maximum and relatively invariant carbon intensity and sp^3 content, and an extremely thin (≤ 1 nm) mostly sp^2 hybridized surface layer [41] is also attributed to the aforementioned unique characteristics of the TEM/EELS hybrid method. In addition to the through-thickness analysis of carbon hybridization, the foregoing method can also provide accurate measurements of the thickness of ultrathin films. For instance, by scanning across the cross section of a Si/*a*-C/Cr stack, the interface of the crystalline Si substrate with the intermixing layer of the *a*-C film can be determined by the first appearance of the C K-major edge peak at 285 eV, whereas the point where the $L_{2,3}$ edge at 99 eV of Si first disappears from the EELS spectrum defines the thickness of the intermixing layer. Similarly, the point where the C K-major edge peak vanishes can be used to determine the total *a*-C film thickness. Beyond this point, only the Cr $L_{2,3}$-major edge peak associated with the Cr capping layer can be detected in the range of 575–584 eV. This methodology of integrating TEM with EELS to ascertain the thickness of the intermixing, bulk, and surface

layers as well as the overall *a*-C film and underlayer thicknesses was further elaborated in a recent study [82]. Fig. 10(b) shows depth profiles of the normalized carbon intensity and the sp^3 hybridization ascertained from the C K-edge EELS spectrum of a Si/*a*-C/Cr stack. The layer interfaces, which define the thickness of the respective layers comprising the *a*-C film, were identified by an established method [81].

NMR spectroscopy has also been used to determine the composition of carbon films, because it provides separate peaks for the sp^2 and sp^3 hybridization states. For example, a 66-ppm chemical shift between sp^2-graphite and sp^3-diamond and 75% sp^3 content were determined from the ^{13}C NMR of cathodic arc *a*-C films [233]. Moreover, the carbon–carbon bonding in *a*-C thin films was determined by combining ^{13}C NMR with EELS [234], and the calculated sp^2 and sp^3 fractions were found to be in agreement with the findings of the previous study. In addition to *a*-C films, NMR spectroscopy has been extensively used to characterize the composition of *a*-C:H films [87, 88, 235–238].

Effect of deposition parameters on thickness, structure and composition of amorphous carbon films synthesized by FCVA

As illustrated in Fig. 11, the FCVA is a multiple input–output film deposition process. A number of parametric studies have been conducted to examine the dependence of the surface roughness, thickness, structure, composition, and tribomechanical properties of FCVA-deposited *a*-C films on key process parameters. These parameters can be categorized as input parameters, which can be independently controlled during film growth, and as output parameters, which can be tailored by accordingly adjusting the input parameters.

One of the most important deposition parameters is the ion energy, which is controlled by the substrate bias voltage. Accurate control of the ion energy is critical to the film quality. For instance, relatively high ion energy induces intense ion bombardment on the growing film surface, which is conducive to the development of a highly compressive mechanical environment that results in film densification and preferential sp^3 hybridization. However, intense ion bombardment can also be detrimental to the film's quality because it may lead to resputtering and graphitization due to the instigation of thermal spikes. This explains the discrepancies in the optimum ion energy reported in the literature. For example, the growth of *a*-C films with optimum properties (i.e., sp^3 content, compressive stress, elastic modulus, and hardness) has been reported for an ion energy equal to 100 eV [186], 120 eV [113], and 140 eV [103, 211], or in the ranges of about 20–40 eV [10], 75–85 eV [17], and 100–150 eV [15, 195]. This variation in the optimum ion energy may be attributed to the fact that the true ion energy is not only controlled by the substrate bias voltage but also by other process parameters, such as the intrinsic plasma ion energy (e.g., ~ 10 to 20 eV for CVA [39, 115]), the plasma potential, and the substrate temperature. Indeed, a transition from very high sp^3-content tetrahedral amorphous carbon (*ta*-C) to *a*-C has been reported for ion energy equal to 90 and 140 eV and a respective substrate temperature of ~ 200 and 140 °C [115].

The ion incidence angle is another important process parameter, especially in high-ion-energy film depositions where the intense ion bombardment can roughen the film surface. In these situations, it is advantageous to continuously vary the ion incidence angle during film growth at a given ion energy. Occasionally, the deposition is performed at grazing angles, a method known as oblique deposition [239]. The deposition rate, topography, thickness, and structure of ultrathin *a*-C films deposited by the FCVA method have been shown to exhibit a strong dependence on the ion incidence angle [97]. More specifically, increasing the ion incidence angle (defined as the angle of the line of ion incidence with the normal to

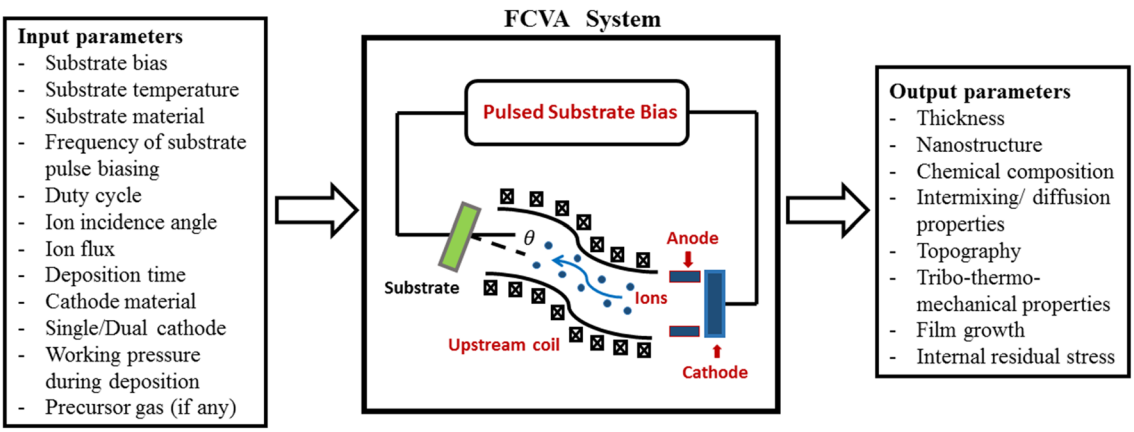

Figure 11: Key input and output parameters of an FCVA system.

the substrate surface) has been found to cause film thinning; however, increasing the ion incidence angle beyond 45° did not reduce the surface roughness and did not increase the sp^3 fraction of the film. Therefore, in terms of the surface smoothness, thickness, and sp^3 hybridization, the main inference derived from the former study is that the optimum incidence angle for FCVA deposition is 45°. In another investigation, affirming the findings of the foregoing study [97], a sharp decrease in the sp^3 content of PLD-grown *a*-C films was observed for incidence angles greater than 45° [239]. Film surface roughening and a decrease in sp^3 content leading to softening of approximately 60- to 120-nm-thick *a*-C films deposited by pulsed CVA was encountered with increasing ion incidence angle [240]. In addition, higher film deposition rates were instigated with the deposition angle decreasing from 70 to 0° (normal incidence). A significant decrease of the internal stresses of *a*-C films deposited by FCVA was reported for relatively high incidence angles attained by substrate tilting, in conjunction with the decrease of the sp^3 content and hardness [117, 241]. These observations can be explained by delving into the dependence of the evolution of the carbon film's structure on the ion incidence angle. Energetic ions at nearly normal incidence can more effectively penetrate the soft sp^2-rich surface layer than at grazing incidence angles, inducing densification and a compressive mechanical environment that is favorable to sp^3 hybridization [231]. Thus, depending on the specific application, the ion incidence angle can be tuned to tailor the film thickness and properties. For instance, when depositing *a*-C films on magnetic disk media, a relatively high ion incidence angle (highly oblique deposition) is preferred to minimize carbon intermixing with the magnetic layer and preserve the magnetic properties, whereas for magnetic head media, nearly normal incidence deposition is preferable. As the miniaturization of magnetic storage devices has progressed, overcoat thinning to thickness levels of ~ 2 nm has revealed an optimum ion incidence angle of 10° for magnetic head media [53, 206].

The duty cycle of the substrate bias voltage is another key input parameter controlling the film growth process. For example, a 65% duty cycle of substrate biasing implies that the bias voltage is on for 65% of the time period during which the resulting intense ion bombardment (depending on the magnitude of the negative substrate bias voltage) favors direct and recoil implantation, densification, and resputtering, whereas for 35% of the pulse period the bias voltage is off during which the ion energy is low (~ 10 to 20 eV for carbon plasma [39, 115]) and the dominant process is deposition. The integration of low-energy deposition with high-energy implantation process steps that result in a hybrid microstructure encompassing film deposition onto a substrate in conjunction with the formation of an intermixing layer intertwined between the deposited film and the substrate is schematically shown in Fig. 12(A). Various thin-film characterization techniques have revealed a strong effect of the duty cycle of substrate biasing on the structure, hybridization, thickness, and surface morphology of FCVA-deposited *a*-C films, showing that a 65% duty cycle produces the smoothest and thinnest films with relatively high sp^3 content [52]. Because high smoothness and very small thickness of the *a*-C films used as protective overcoats in magnetic storage are critically important, optimizing the bias duty cycle to produce extremely smooth, ultrathin *a*-C films is imperative in contemporary information storage technologies, such as the HAMR technology. While a 50% duty cycle has been reported for maximum film hardness [186], hardness measurements were not obtained for bias duty cycles above 50% and, thus, definitive statements about an optimum bias duty cycle cannot be deduced. In addition to the bias duty cycle, the frequency of substrate pulse biasing can also affect the film properties. Indeed, a decrease of the internal stress of *a*-C and *a*-C:Al films by as much as 85% was found for film depositions performed at pulse frequencies in the range of 600–1000 Hz; nevertheless, a decrease in wear resistance was also observed with increasing pulse frequency [242]. Moreover, it was discovered that while incorporating a metal, such as Al, into the *a*-C matrix may reduce the film stress, it can also increase the film roughness.

The film thickness is a strong function of the flux of film precursors (C^+ ions in the case of *a*-C films) and the deposition time. The typical C^+ ion flux rate measured right above the substrate holder of an FCVA system is equal to 1.48×10^{19} ions/m^2·s [54]. Similar C^+ ion fluxes have been reported in other carbon film growth studies that used FCVA deposition [41, 64, 97, 98]. In addition, the C^+ ion fluency has been observed to strongly affect the film structure [243], but not the *a*-C/Si substrate interface [244]. Indeed, insignificant changes in the film/substrate interface have been observed for various deposition times, i.e., by varying the total C^+ ion fluence [244]. For a fixed C^+ ion flux, the thickness of ultrathin films is directly proportional to the deposition time. Specifically, for FCVA-deposited *a*-C films of thickness ~ 1 to 2 nm, the typical deposition time is equal to ~ 6 s [53, 81]. This extremely short time elevates the importance of stable arcing with the instigation of the deposition process. This has been achieved by using a "cusp" configuration of the magnetic field in which the magnetic field lines around the anode intersect those of the cathode at 90°, stabilizing the arc current and maintaining a continuous electron flux from the cathode to the anode [54]. For a deposition time less than 6 s, effective control of plasma ignition is challenging, but more importantly, the resulting *a*-C film structure consists only of intermixing and surface layers, i.e., the sp^3-rich bulk layer which is responsible for the excellent tribomechanical properties of the *a*-C film does not form. A compilation of the optimized deposition parameters used to synthesize high-quality *a*-C films by the CVA method is given in Table 2.

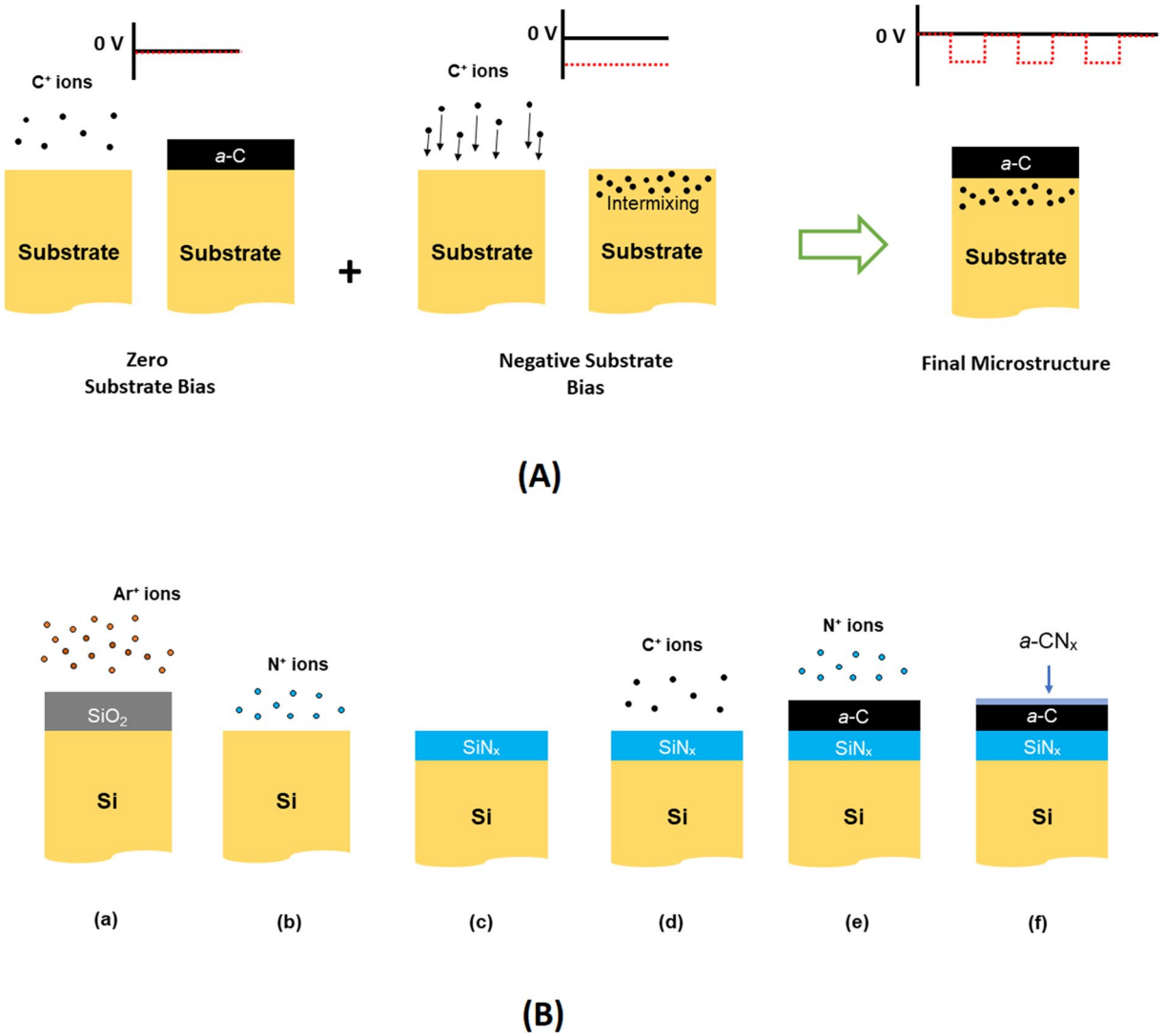

Figure 12: (A) Schematic demonstrating the integration of conventional sputtering-based deposition (during zero substrate bias voltage) with conventional ion implantation into the substrate forming an intermixing layer (during negative substrate bias voltage) steps in FCVA-synthesized ultrathin *a*-C films. (B) Experimental procedure for depositing an *a*-C film and a SiN_x underlayer and post-deposition tailoring of the *a*-C film microstructure (particularly, the surface layer) to enhance its wear resistance and durability. (Adapted from Ref. [82]) (a) A Si(100) wafer is partitioned into 5×5 mm^2 sections and the native oxide layer is removed by Ar^+ ion sputter etching. (b) Nitrogenation of the Si substrate by N^+ ion bombardment in a rf sputtering system. (c) Formation of an ultrathin SiN_x underlayer on top of the Si substrate. (d) Deposition of an ultrathin *a*-C film using a custom-made FCVA system. (e) Nitrogenation of the surface layer of the *a*-C film by N^+ ion bombardment in a rf sputtering system. (f) Final *a*-CN_x/*a*-C/SiN_x/Si stack.

Structural stability of amorphous carbon films synthesized by FCVA

The significance of the structural stability of *a*-C overcoats in elevated-temperature applications has generated notable research efforts aimed at identifying changes in the structure, composition, and tribomechanical properties of *a*-C films exposed to various temperatures. Particular attention has been given to the structural stability of *a*-C films under highly localized, rapid heating conditions, such as those encountered in laser photonics and HAMR drives. Consequently, rapid thermal annealing (RTA) studies have been carried out to explore the structural stability of *a*-C films at various temperatures. During the RTA treatment, the coated sample is rapidly heated to an elevated temperature, kept at that temperature for a certain period of time and, finally, cooled down to room temperature. Some of the earlier thermal studies of overcoat films were performed with relatively thick (~ 500 nm) *a*-C films and temperatures as high as 1000 °C. For such thick films synthesized by rf plasma decomposition of acetylene, sp^3-to-sp^2 rehybridization was observed after heating at temperatures > 390 °C for 4 h in vacuum and complete graphitization at temperatures > 590 °C [169]. Similarly, heating of DLC films grown by direct ion-beam

TABLE 2: Optimal deposition parameters of *a*-C films synthesized by the CVA method.

Deposition parameter	Magnitude/sub-type	References
Duty cycle of substrate bias voltage	65%	[52]
	60%	[125, 205]
	50%	[186]
Pulse frequency of substrate biasing	600–1000 Hz	[242]
	25 kHz	[54]
Substrate bias voltage for optimized tribo-thermo-mechanical properties	– 120 V	[113]
	– 90 V	[125]
	– 100 V	[186]
	– 80 V	[82, 99]
	– 140 V	[103, 211]
	– 75 to – 85 V	[17]
	– 75 V	[81]
	– 20 to – 40 V	[10]
	– 100 to – 150 V	[15, 195]
Substrate-plasma beam inclination for optimized tribo-thermo-mechanical properties	45°	[97]
	59–77°	[240]
	10°	[53, 82, 206]
	0° (normal incidence)	[117, 239, 241]
Substrate-plasma beam inclination for minimal internal residual stress	60°	[97, 241]
	75°	[117]
Species selective biasing applied to the substrate	Applied via a computer controlled bias amplifier	[57, 61]
	Software controlled (LabView)	[56, 59, 60]
Working pressure	$\sim 5 \times 10^{-7}$ Torr	[53, 81, 82, 100, 126, 206]
	$\sim 5 \times 10^{-8}$ Torr	[121, 122]
	$\sim 7.5 \times 10^{-8}$ Torr	[70]
	$\sim 8 \times 10^{-8}$ Torr	[124]
	$\sim 4.5 \times 10^{-6}$ Torr	[244]
	$\sim 3 \times 10^{-6}$ Torr	[205]
Ion fluency	5×10^{21} ions/m^2	[243]
Ion flux	1.48×10^{19} ions/m^2·s	[52–54, 64, 81, 97]

deposition at a temperature above 500 °C for 2 min in nitrogen atmosphere resulted in graphitization, as revealed by the presence of a crystalline graphite peak in the Raman spectra [245]. Interestingly, thinner carbon films have been found to exhibit greater rehybridization resistance. For example, 30- and 70-nm-thick *ta*-C films deposited on silicon exhibited significant sp^3-to-sp^2 rehybridization only after heating at 1100 °C for 20 min in an inert atmosphere and relaxation of the intrinsic compressive stress with minimal structural change in the 600–700 °C temperature range [246]. In another similar study, 70-nm-thick *ta*-C films (85% sp^3 content) synthesized by the CVA method and heated at temperatures between 300 and 850 °C for 15 min demonstrated graphitization only at the near-surface region, which did not affect the mechanical properties up to a temperature of 700 °C [247]. Complete surface graphitization of thin *a*-C films heated above 900 °C has also been detected by near-edge X-ray absorption and X-ray photoemission spectroscopy [248].

Moreover, annealing of multilayer *a*-C films consisting of alternating high/low-density *a*-C layers at 600 °C in vacuum decreased the intrinsic compressive stress in the films [249]. It was also reported that *a*-C film deposition using high energy ions (corresponding to a – 720 V bias voltage) culminated in dynamic annealing, producing a similar thermal effect as that of thermal annealing by increasing the overall sp^2 content of the multilayer film assembly. However, the physics of dynamic annealing, which is intrinsic to high energy ion bombardment, is radically different from that of substrate heating to an elevated temperature during film deposition. This can be explained by considering that dynamic annealing induces sp^3-to-sp^2 rehybridization through thermal spikes, whereas the degradation of sp^3 bonding at high substrate temperatures is a consequence of thermally induced atomic diffusion of implanted carbon towards the substrate surface. Since this diffusion process relaxes the film stress, it inhibits the development of a compressive mechanical environment, which is conducive to sp^3 hybridization. Indeed,

a strong transition to sp^2-dominated *a*-C film growth has been found for substrate temperatures above 200 °C [115], consistent with simulation results revealing film amorphization at 200 °C [250].

Despite valuable insight into the thermal stability of carbon films at elevated temperatures and inert environments derived from earlier studies, profound changes in the film microstructure may be encountered in oxidizing atmospheres. Indeed, heating of 70-nm-thick *ta*-C films deposited by FCVA at temperatures in the range of 100–450 °C for 35 min in an oxidizing atmosphere under low or high vacuum conditions revealed significant differences in the Raman spectra at temperatures > 300 °C and insignificant changes in the microstructure, thickness, compressive stress, and hardness of the films heated up to 400 °C in both low and high vacuum [251]. In another Raman study [222], an increase of the sp^2 content of FCVA-deposited 40-nm-thick *ta*-C films was found with the increase of the substrate temperature in the range of 25–400 °C. This finding may be attributed to the enhancement of the carbon atom diffusivity by the supplied thermal energy that relieved the intrinsic compressive stress, consecutively culminating in sp^2 hybridization. Similar findings were observed in a Raman study of 50-nm-thick *ta*-C films with the increase of temperature above 250 °C [252]. In recent thermal studies of carbon films, the focus was on ultrathin (< 5 nm thick) *a*-C films, presumably because of the increasing usage of these films as protective overcoats in several leading technologies. Consequently, a decrease of the reflectivity of 4.5-nm-thick sputtered *a*-C films, which correlates to the film density and sp^3 content, commenced at a temperature of 220 °C due to pulsed laser irradiation [253]. The graphitization of PECVD-deposited carbon films during extremely rapid heating (~ 10^6 K/s) at a temperature of ~ 450 °C [177] demonstrates that these films destabilize and oxidize at elevated temperatures, such as those encountered in HAMR and photonic applications. Hydrogen depletion, sp^2 cluster enlargement, and augmentation of the carbon network ordering characterized the structural destabilization of ultrathin *a*-C:H films at RTA temperatures > 450 °C and ambient air [254].

The superior structural stability of ultrathin carbon films synthesized by FCVA over PECVD has been demonstrated under conditions of rapid heating (1 s) at a high temperature (650 °C) or prolonged heating (~ 1 h) at a moderately high temperature (~ 227 °C) and ambient air [110, 112]. The structural and topographical changes and the degradation of the tribological properties of 2-nm-thick carbon films produced by magnetron sputtering caused by rapid (1 s) heating at temperatures > 400 °C were attributed to the lower sp^3/sp^2 ratio of the sputtered films; nevertheless, no effect was found for FCVA carbon films of similar thickness [151]. In another thermal study [255], however, the thermal robustness of 3-nm-thick carbon films grown by CVD was found to be better than that of FCVA carbon films of similar thickness. This result was attributed to the higher sp^3 content of the CVD films, which strongly affects the tribo-thermo-mechanical properties of *a*-C films.

Thermal studies have also been performed with bilayer films consisting of an *a*-C overcoat and an underlayer acting as an adhesion and corrosion-resistant layer. For instance, the structural stability of ultrathin FCVA *a*-C films with SiN_x, NiCr, or TaO_x underlayers was demonstrated under conditions of prolonged (30–90 min) heating at 250 and 350 °C in inert atmosphere [81, 82] and in RTA molecular dynamics simulations [250]. The foregoing studies confirmed that nanometer-thick *a*-C films synthesized under optimal FCVA conditions resulting in relatively high sp^3 content (~ 60%) demonstrate structural stability up to a temperature in the range of 200–250 °C.

Some interesting phenomena were encountered in the course of exploring the structural stability of *a*-C films during RTA under inert atmosphere or vacuum conditions. Specifically, heating of Si/NiFe/*a*-C stacks at 650 °C for 2.5 min in Ar atmosphere led to the formation of planar graphene (PG) and orbicular graphitic carbon (OGC) at the surface of the *a*-C film and the growth of pyramidal $NiSi_x$ nanocrystals extending into the Si substrate [256]. This hybrid film comprising PG, OGC, and $NiSi_x$ nanostructures has high potential for widespread nanoelectronics applications. Moreover, the conversion of the low-sp^3 surface layer of FCVA *a*-C films to graphene is desirable because it enhances the tribological properties [257, 258]. In a completely different application involving thermal treatment, Ga nanospheres were formed at the surface of FCVA *a*-C films implanted with Ga after thermal annealing at 500 °C for 1 h in vacuum, which has important applications in photonics [259]. This phenomenon was attributed to Ga supersaturation of the *a*-C matrix, resulting in surface segregation of the Ga during annealing.

Underlayer-induced enhancement of film properties

Overcoat applications in high-temperature environments often necessitate the incorporation of an ultrathin underlayer between the overcoat and the substrate to enhance interfacial adhesion and to prevent elemental diffusion and oxidation of the substrate material. An underlayer that possesses high density, refractory properties, and good adhesion characteristics is extremely beneficial because it augments the overall performance of the overcoat. This is because a high-density matrix prevents carbon and other elemental migration and percolations through the matrix, the refractory properties ensure thermal stability at elevated temperatures, whereas a high interfacial adhesion aids to strongly bond the overcoat to the underlying material. This becomes particularly critical in applications where contact

tractions and mismatches of the elastic–plastic properties and thermal expansion characteristics produce large stress and strain gradients at the overcoat/substrate interface, which frequently lead to overcoat delamination. It is noted that the intermixing layer of overcoats synthesized under conditions conducive to subplantation is not due to elemental diffusion.

Figure 12(B) shows a schematic of an experimental procedure used to incorporate an underlayer between the overcoat and the substrate [82]. The process flow displays the sequential steps of forming a SiN_x underlayer by reactive rf sputtering, followed by the deposition of an *a*-C overcoat by the FCVA method. The last step in the process illuminates an innovative direction wherein the wear characteristics of the surface layer can be improved by nitrogenation to form an *a*-CN_x film. This post-deposition nitrogenation method is in stark contrast to the formation of *a*-CN_x films using a high-pressure nitrogen jet in the vicinity of the cathode arc spots from which the plasma originates [260]. Furthermore, to enhance the wear resistance and hardness of the near-surface region of *a*-C films, different ions, such as Al, Si, Ti, W, and Hf, can be implanted into the overcoat's surface by either direct ion implantation or PIIID, as demonstrated in previous studies [187, 203]. The foregoing studies established the effectiveness and positive effect of the latter post-processing methods in improving the overall tribomechanical properties of the overcoat. The initial success with embedding these ions into the carbon matrix using different ion implantation techniques motivates further examination in this direction with experiments targeting different metal/ceramic constituents and optimizing implantation parameters, e.g., size of implant species, ion dose, and average kinetic energy of the impinging ions.

In some technologically innovative designs [261], a metallic underlayer may be used in conjunction with an adhesion layer to enhance the protection of vital components, such as the WP and the NFT elements of a HAMR head. The metallic underlayer may comprise one or more metals (e.g., Pt, Pd, Ru, Ir, Cr, Ti, Ta, or other transition metals and metal combinations thereof) and must demonstrate low solubility to the underlying material, good oxidation and corrosion resistance, high melting point, decent optical properties, and thickness in the range of 0.5–5 nm. Heating at 400 °C for 48 h in vacuum revealed that an optimum stack configuration is *a*-C/Cr/Ir of 2:2:2.5 nm in thickness [261]. Other promising underlayers that exhibit improved functional characteristics are AuCu, NiCr, NiAl [261], TaO_x [81], and CrN_x [262].

In addition to metal and alloy underlayers, significant research has been devoted towards the development of Si-based underlayers for ultrathin *a*-C overcoats, particularly, SiN_x underlayers [81, 82, 119–126]. This is a consequence of the high hardness and corrosion resistance [120, 123] and enhanced adhesion of SiN_x [122, 124, 125] to carbon and metal alloys than most other materials in conjunction with the easiness of forming an ultrathin SiN_x underlayer. In fact, an atomically thin SiN_x underlayer can proliferate the overcoat's bonding strength and also augment sp^3 hybridization, increase the oxidation and corrosion resistance, and improve the tribological properties of *a*-C overcoats [120, 126]. Additionally, an ultrathin SiN_x underlayer can play a dual role in elevated temperature, inert environments by maintaining the structural stability and interfacial adhesion of the *a*-C overcoat, and preventing carbon diffusion into the substrate [82]. Further studies are needed to prove whether the foregoing desirable attributes of an ultrathin SiN_x underlayer can also be encountered in high temperature, oxidative environments.

Studies concerned with the effect of an underlayer on the tribological properties of layered stacks have shown that, in addition to the high sp^3 fraction and strong interfacial adhesion, it is necessary to optimize the thicknesses of both the *a*-C overcoat and the SiN_x underlayer. This is dictated by the objective to attain low friction and high wear resistance and the fact that tuning the interface microstructure by varying the *a*-C and SiN_x thicknesses is critical due to the scale dependence of the tribological behavior [121]. The superior tribological properties of a layered *a*-C/SiN_x coating compared to those of a single *a*-C coating of equal thickness have been attributed to the chemistry of the *a*-C/SiN_x interface and the high affinity of SiN_x towards carbon, metals, and ceramics [122, 124, 126].

In deposition methods where the film precursors are energetic ions, the formation of an intermixing layer can play the role of an adhesion underlayer, which can be adjusted to display desirable functional attributes. For instance, the subplantation process in energetic C^+ ion bombardment leads to the formation of an intermixing layer consisting of carbon and substrate elements [205, 207, 263, 264]. Additionally, the energetic particle bombardment can also be used to modify the structure and properties of the underlayer prior to the deposition of the overcoat. As an example, 350-eV C^+ ion bombardment of a Si underlayer deposited on a composite Al_2O_3–TiC substrate prior to the growth of an *a*-C overcoat enhanced the interfacial adhesion in the *a*-C/Si/Al_2O_3–TiC stack through the formation of Si–C, Al–O–Si, and Si–O–C bond networks, which augmented the wear life and durability of the *a*-C overcoat [207]. Similar findings and improved tribological properties were reported for the case of direct C^+ ion bombardment onto an Al_2O_3–TiC substrate without depositing a Si or Si-based underlayer between the *a*-C overcoat and the substrate [205], suggesting that the formed intermixing layer played a similar role with the Si underlayer used elsewhere [207]. The enhancement of the interfacial adhesion through the formation of a composite Si-Al-C underlayer via the foregoing pretreatment process is considered to be the main factor for the improved wear characteristics of this type of overcoat assembly [263]. Moreover, a 350-eV C^+ ion

bombardment of the substrate surface before the deposition of the *a*-C overcoat has been reported to enhance the corrosion resistance of the layered stack by aiding to the formation of a dense intermixing layer and the increase of the sp^3 content [264].

The formation of an intermixing layer by the subplantation process [231] is commonly encountered in deposition processes where the film precursors are energetic particles. However, an intermixing layer may also form via heating. The supplied thermal energy enables carbon atoms to overcome the energy barrier for diffusion into the bulk material. While the intermixing layer enhances the interfacial strength and provides a gradual transition from the overcoat to the substrate properties that reduces the local large stress/strain gradients caused by thermal expansion coefficient and lattice mismatches, it also changes the substrate properties, which may not be desirable in certain applications. For example, the intermixing layer of a carbon overcoat can alter the magnetic characteristics of the FeNi alloy used to fabricate the WP of magnetic heads. Consequently, a prominent feature of an underlayer is that the overcoat's intermixing layer is fully contained within the bulk of the underlayer. Thus, one of the main challenges is that the underlayer is sufficiently thick to prevent substrate alloying by the subplantation process during overcoat deposition and by diffusion during heating, but also as thin as possible to avoid increasing the physical space between the read/write element of the head and the magnetic medium of the hard disk.

Conclusions and outlook

Among all of the film deposition methods used to synthesize thin *a*-C films, the CVA technique demonstrates the highest potential because it allows modulation of the film's structure through the adjustment of key process parameters, such as the ion energy (substrate bias voltage), ion incidence angle, and duty cycle of substrate biasing (which controls direct/recoil implantation and deposition), with additional desirable characteristics including low-temperature deposition, effective plasma manipulation, macro/microparticle filtering, and stable plasma arcing. Continuous miniaturization of microelectromechanical devices requiring functional overcoats has prompted the development of ultrathin films with thicknesses only a few nanometers. This dramatic decrease in film thickness has been attended by advances in high-resolution imaging and characterization techniques and inventions in instrumentation, mainly particle filtering and duct designs, species selective biasing, oblique deposition, and dual cathode deposition. These innovations have enabled a rapid progress in ultrathin film synthesis, especially for applications where the device performance greatly depends on maintaining the quality and integrity of the protective film in hot and oxidative environments. An important advance towards the foregoing progress is the development of hybrid coatings consisting of an *a*-C overcoat and an underlayer (e.g., Si, SiN_x, NiCr, and TaO_x), which prevents elemental interdiffusion, enhances interface bonding, and increases the oxidation and corrosion resistance.

Although the CVA method has been mostly used to deposit ultrathin films on planar and low-curvature components, there is a great potential to extend the use of this method in 3D printing for nanoscale surface engineering, particularly the fabrication of nanostructures for semiconductor applications. The successful integration of CVA with lithography is an interesting outlook that can revolutionize the landscape of surface nanostructuring. Another exciting prospect is the design of CVA systems with integrated multiple plasma streams to attain hybrid materials, e.g., coating metallic substrates with high-temperature alloys (MCrAlY, M = Fe, Ni, Co). The incorporation of underlayers has been an area of active research both in the scientific community and the magnetic recording industry. In that regard, the co-deposition of carbon and rare earth elements (e.g., Ru and Rh) or the deposition of ultrathin underlayers containing rare earth elements has been garnering significant attention lately. Importantly, since Rh exhibits a thermal expansion coefficient similar to those of Fe and Co, it can be used to reduce the interfacial stresses due to the thermal expansion mismatch between the *a*-C overcoat and Fe- or Co-based alloys. Further explorations could be channeled towards synthesizing films and underlayers with different compositions and ascertaining which combinations offer the most versatile range of properties for specific applications.

Nonetheless, despite the numerous advantages of CVA systems there are still certain shortcomings that must be overcome before broadening the application range of this novel method. In the case of thin and ultrathin *a*-C films deposited by CVA, the film structure consists of three layers, i.e., intermixing, bulk, and surface layers, from which, the sp^3-rich bulk layer controls the overall tribo-thermo-mechanical properties of the film. However, after the extensive research devoted to improve the properties of the bulk layer, the focus has been gradually shifting towards the sp^2-rich surface layer, which is relatively soft and the first to oxidize and wear out due to intermittent surface contact during the operation of contact-mode devices. To offset this shortcoming, nitrogenation or other case hardening techniques can be used to harden the surface layer of the *a*-C film. Because the surface layer represents the first barrier against tribomechanical and oxidation/corrosion damage, optimizing the composition of the surface layer by alloying with key elements is critical to enhancing its properties. Another challenge is coating large components with the CVA method. Scaling up from the nanometer-thick films and small substrates to thicker films and especially much larger components is challenging because of the nonlinear scale dependence of the deposition process dynamics. An important issue affecting the film uniformity is that the ion flux distribution exhibits a gradual decay in the radial direction. A plausible solution is to use a magnetic field to adjust the ion flux in the proximity of the coated object, which

requires iterative design improvements in the instrumentation of the CVA system. Similar to the magnetic field used to condense the plasma beam between the cathode and the substrate, a magnetic field can be applied to uniformly spread the plasma beam near the substrate surface to improve the uniformity in the deposited film in the radial direction. This would be particularly beneficial for uniformly coating large components and surface nanostructuring of larger wafers used in microelectronics or other applications involving fabrication of microdevices. The general outlook for CVA remains that while nanoscale is going to be absolutely paramount going forward, with the surface layer playing a predominant role in the near future, scalability limitations must be overcome to broaden the application range of this novel coating method.

Acknowledgments

This work was supported by Western Digital Technologies, Inc. The TEM/EELS studies were performed at the National Center for Electron Microscopy, Molecular Foundry, Lawrence Berkeley National Laboratory (Proposal No. 5661). The work at the Molecular Foundry was supported by the Office of Science, Office of Basic Energy Sciences, of the U.S. Department of Energy under Contract No. DE-AC02-05CH11231.

Data availability

Data can be made available upon reasonable request to the corresponding author.

Declarations

Conflict of interest The authors declare no competing interests.

References

1. I.G. Brown, Cathodic arc deposition of films. Annu. Rev. Mater. Sci. **28**, 243 (1998)
2. J. Robertson, Ultrathin carbon coatings for magnetic storage technology. Thin Solid Films **383**, 81 (2001)
3. M.K. Fung, K.H. Lai, C.Y. Chan, I. Bello, C.S. Lee, S.T. Lee, D.S. Mao, X. Wang, Mechanical properties and corrosion studies of amorphous carbon on magnetic disks prepared by ECR plasma technique. Thin Solid Films **368**, 198 (2000)
4. R. Hauert, An overview on the tribological behavior of diamond-like carbon in technical and medical applications. Tribol. Int. **37**, 991 (2004)
5. A. Erdemir, C. Donnet, Tribology of diamond-like carbon films: recent progress and future prospects. J. Phys. D **39**, R311 (2006)
6. C.S. Bhatia, S. Anders, I.G. Brown, K. Bobb, R. Hsiao, D.B. Bogy, Ultra-thin overcoats for the head/disk interface tribology. ASME J. Tribol. **120**, 795 (1998)
7. T. Xu, L. Pruitt, Diamond-like carbon coatings for orthopaedic applications: an evaluation of tribological performance. J. Mater. Sci. **10**, 83 (1999)
8. A. Grill, Tribology of diamondlike carbon and related materials: an updated review. Surf. Coat. Technol. **94–95**, 507 (1997)
9. B. Bhushan, Chemical, mechanical and tribological characterization of ultra-thin and hard amorphous carbon coatings as thin as 3.5 nm: recent developments. Diam. Relat. Mater. **8**, 1985 (1999)
10. D.R. McKenzie, D. Muller, B.A. Pailthorpe, Compressive-stress-induced formation of thin-film tetrahedral amorphous carbon. Phys. Rev. Lett. **67**, 773 (1991)
11. P.H. Gaskell, A. Saeed, P. Chieux, D.R. McKenzie, Neutron-scattering studies of the structure of highly tetrahedral amorphous diamondlike carbon. Phys. Rev. Lett. **67**, 1286 (1991)
12. J.C. Angus, C.C. Hayman, Low-pressure, metastable growth of diamond and "diamondlike" phases. Science **241**, 913 (1988)
13. A. Grill, B.S. Meyerson, Development and status of diamond-like carbon, in *Synthetic Diamond-Emerging CVD Science and Technology*, ed. by K.E. Spear, J.P. Dismukes (Wiley, New York, 1994), pp.91–146
14. H.-S. Zhang, K. Komvopoulos, Surface modification of magnetic recording media by filtered cathodic vacuum arc. J. Appl. Phys. **106**, 093504 (2009)
15. J. Ishikawa, Y. Takeiri, K. Ogawa, T. Takagi, Transparent carbon film prepared by mass-separated negative-carbon-ion-beam deposition. J. Appl. Phys. **61**, 2509 (1987)
16. W. Lu, K. Komvopoulos, Dependence of growth and nanomechanical properties of ultrathin amorphous carbon films on radio frequency sputtering conditions. J. Appl. Phys. **86**, 2268 (1999)
17. S. Xu, B.K. Tay, H.S. Tan, L. Zhong, Y.Q. Tu, S.R.P. Silva, W.I. Milne, Properties of carbon ion deposited tetrahedral amorphous carbon films as a function of ion energy. J. Appl. Phys. **79**, 7234 (1996)
18. A.A. Voevodin, M.S. Donley, Preparation of amorphous diamond-like carbon by pulsed laser deposition: a critical review. Surf. Coat. Technol. **82**, 199 (1996)
19. W. Lu, K. Komvopoulos, Nanotribological and nanomechanical properties of ultrathin amorphous carbon films synthesized by radio frequency sputtering. ASME J. Tribol. **123**, 641 (2001)
20. A. Anders, Physics of plasma-based ion implantation & deposition (PBIID) and high power impulse magnetron sputtering (HIPIMS): a comparison. Phys. Status Solidi A **205**, 965 (2008)
21. S. Anders, I.G. Brown, C.S. Bhatia, D.B. Bogy, Cathodic arc deposited diamond-like carbon films for head-disk tribology applications. Data Storage **4**, 31 (1997)

22. A. Anders, Energetic deposition using filtered cathodic arc plasmas. Vacuum **67**, 673 (2002)
23. A.H. Lettington, Applications of diamond-like carbon thin films, in *Thin Film Diamond*, ed. by A.H. Lettington, J.W. Steeds (Springer, Dordrecht, 1994), pp.117–126
24. T.S. Santra, T.K. Bhattacharyya, P. Patel, F.G. Tseng, T.K. Barik, Diamond, diamond-like carbon (DLC) and diamond-like nanocomposite (DLN) thin films for MEMS applications, in *Microelectromechanical Systems and Devices*, ed. by N. Islam (In Tech, Rijeka, 2012), pp.459–480
25. A. Grill, Diamond-like carbon coatings as biocompatible materials—an overview. Diam. Relat. Mater. **12**, 166 (2003)
26. V. Mehta, J.S. Cooper, Review and analysis of PEM fuel cell design and manufacturing. J. Power Sources **114**, 32 (2003)
27. J.Y. Sze, B.K. Tay, Carbon ion implantation of ultra-high molecular weight polyethylene using filtered cathodic vacuum arc with substrate pulse biasing. Surf. Coat. Technol. **200**, 4104 (2006)
28. D.P. Dowling, P.V. Kola, K. Donnelly, T.C. Kelly, K. Brumitt, L. Lloyd, R. Eloy, M. Therin, N. Weill, Evaluation of diamond-like carbon-coated orthopaedic implants. Diam. Relat. Mater. **6**, 390 (1997)
29. H. Tsai, D.B. Bogy, Characterization of diamondlike carbon films and their application as overcoats on thin-film media for magnetic recording. J. Vac. Sci. Technol. A **5**, 3287 (1987)
30. C. Casiraghi, J. Robertson, A.C. Ferrari, Diamond-like carbon for data and beer storage. Mater. Today **10**, 44 (2007)
31. E.M. Moser, R. Urech, E. Hack, H. Künzli, E. Müller, Hydrocarbon films inhibit oxygen permeation through plastic packaging material. Thin Solid Films **317**, 388 (1998)
32. M.H. Kryder, E.C. Gage, T.W. McDaniel, W.A. Challener, R.E. Rottmayer, G. Ju, Y.-T. Hsia, M.F. Erden, Heat assisted magnetic recording. Proc. IEEE **96**, 1810 (2008)
33. L.K. Cheah, X. Shi, E. Liu, J.R. Shi, Nitrogenated tetrahedral amorphous carbon films prepared by ion-beam-assisted filtered cathodic vacuum arc technique for solar cells application. Appl. Phys. Lett. **73**, 2473 (1998)
34. J.K. Luo, Y.Q. Fu, H.R. Le, J.A. Williams, S.M. Spearing, W.I. Milne, Diamond and diamond-like carbon MEMS. J. Micromech. Microeng. **17**, S147 (2007)
35. Y. Wu, H. Li, L. Ji, Y. Ye, J. Chen, H. Zhou, Preparation and properties of MoS_2/a-C films for space tribology. J. Phys. D **46**, 425301 (2013)
36. K. Komvopoulos, Surface engineering and microtribology for microelectromechanical systems. Wear **200**, 305 (1996)
37. K. Komvopoulos, Adhesion and friction forces in microelectromechanical systems: mechanisms, measurement, surface modification techniques, and adhesion theory. J. Adhes. Sci. Technol. **17**, 477 (2003)
38. S.R.P. Silva, *Properties of Amorphous Carbon* (INSPEC, London, 2003)
39. J. Robertson, Requirements of ultrathin carbon coatings for magnetic storage technology. Tribol. Int. **36**, 405 (2003)
40. P.R. Goglia, J. Berkowitz, J. Hoehn, A. Xidis, L. Stover, Diamond-like carbon applications in high density hard disc recording heads. Diam. Relat. Mater. **10**, 271 (2001)
41. N. Wang, K. Komvopoulos, The multilayered structure of ultrathin amorphous carbon films synthesized by filtered cathodic vacuum arc deposition. J. Mater. Res. **28**, 2124 (2013)
42. C.A. Davis, G.A.J. Amaratunga, K.M. Knowles, Growth mechanism and cross-sectional structure of tetrahedral amorphous carbon thin films. Phys. Rev. Lett. **80**, 3280 (1998)
43. C.A. Davis, K.M. Knowles, G.A.J. Amaratunga, Cross-sectional structure of tetrahedral amorphous carbon thin films. Surf. Coat. Technol. **76–77**, 316 (1995)
44. M.P. Siegal, P.N. Provencio, D.R. Tallant, R.L. Simpson, B. Kleinsorge, W.I. Milne, Bonding topologies in diamondlike amorphous-carbon films. Appl. Phys. Lett. **76**, 2047 (2000)
45. J. Robertson, Diamond-like amorphous carbon. Mater. Sci. Eng. R **37**, 129 (2002)
46. R.L. Wallace Jr., The reproduction of magnetically recorded signals. Bell Syst. Tech. J. **30**, 1145 (1951)
47. R. Wood, Future hard disk drive systems. J. Magn. Magn. Mater. **321**, 555 (2009)
48. Z.Z. Bandić, R.H. Victora, Advances in magnetic data storage technologies. Proc. IEEE **96**, 1749 (2008)
49. Z.-M. Yuan, B. Liu, T. Zhou, C.K. Goh, C.L. Ong, C.M. Cheong, L. Wang, Perspectives of magnetic recording system at 10 Tb/in^2. IEEE Trans. Magn. **45**, 5038 (2009)
50. X. Wang, K. Gao, H. Zhou, A. Itagi, M. Seigler, E. Gage, HAMR recording limitations and extendibility. IEEE Trans. Magn. **49**, 686 (2013)
51. N. Yasui, H. Inaba, K. Furusawa, M. Saito, N. Ohtake, Characterization of head overcoat for 1 Tb/in^2 magnetic recording. IEEE Trans. Magn. **45**, 805 (2009)
52. J. Xie, K. Komvopoulos, The role of duty cycle of substrate pulse biasing in filtered cathodic vacuum arc deposition of amorphous carbon films. IEEE Trans. Magn. **51**, 3302009 (2015)
53. J. Matlak, K. Komvopoulos, Ultrathin amorphous carbon films synthesized by filtered cathodic vacuum arc used as protective overcoats of heat-assisted magnetic recording heads. Sci. Rep. **8**, 9647 (2018)
54. H.-S. Zhang, K. Komvopoulos, Direct-current cathodic vacuum arc system with magnetic-field mechanism for plasma stabilization. Rev. Sci. Instrum. **79**, 073905 (2008)
55. A. Anders, Cathodic arc sources, in *Cathodic Arcs*, *Springer Series on Atomic, Optical, and Plasma Physics*, vol. 50 (Springer, New York, 2008), pp.299–362
56. N. Pasaja, S. Sansongsiri, S. Intarasiri, T. Vilaithong, A. Anders, Mo-containing tetrahedral amorphous carbon deposited by dual filtered cathodic vacuum arc with selective pulsed bias voltage. Nucl. Instrum. Meth. Phys. Res. B **259**, 867 (2007)

57. S. Sansongsiri, A. Anders, B. Yotsombat, Electrical properties of a-C: Mo films produced by dual-cathode filtered cathodic arc plasma deposition. Diam. Relat. Mater. **17**, 2080 (2008)
58. J.L. Endrino, D. Horwat, A. Anders, J. Andersson, R. Gago, Impact of annealing on the conductivity of amorphous carbon films incorporating copper and gold nanoparticles deposited by pulsed dual cathodic arc. Plasma Process. Polym. **6**, S438 (2009)
59. J.L. Endrino, R. Escobar Galindo, H.-S. Zhang, M. Allen, R. Gago, A. Espinosa, A. Anders, Structure and properties of silver-containing a-C(H) films deposited by plasma immersion ion implantation. Surf. Coat. Technol. **202**, 3675 (2008)
60. A. Anders, N. Pasaja, S. Sansongsiri, Filtered cathodic arc deposition with ion-species-selective bias. Rev. Sci. Instrum. **78**, 063901 (2007)
61. J.L. Endrino, D. Horwat, R. Gago, J. Andersson, Y.S. Liu, J. Guo, A. Anders, Electronic structure and conductivity of nanocomposite metal (Au, Ag, Cu, Mo)-containing amorphous carbon films. Solid State Sci. **11**, 1742 (2009)
62. O.R. Monteiro, M.-P. Delplancke-Ogletree, I.G. Brown, Tungsten-containing amorphous carbon films deposited by pulsed vacuum arc. Thin Solid Films **342**, 100 (1999)
63. O.R. Monteiro, M.-P. Delplancke-Ogletree, R.Y. Lo, R. Winand, I. Brown, Synthesis and characterization of thin films of WC_x produced by mixing W and C plasma streams. Surf. Coat. Technol. **94–95**, 220 (1997)
64. H.-S. Zhang, K. Komvopoulos, Synthesis of ultrathin carbon films by direct current filtered cathodic vacuum arc. J. Appl. Phys. **105**, 083305 (2009)
65. J. Koskinen, A. Anttila, J.-P. Hirvonen, Diamond-like carbon coatings by arc-discharge methods. Surf. Coat. Technol. **47**, 180 (1991)
66. S. Anders, A. Anders, I. Brown, Macroparticle-free thin films produced by an efficient vacuum arc deposition technique. J. Appl. Phys. **74**, 4239 (1993)
67. V.S. Veerasamy, G.A.J. Amaratunga, W.I. Milne, P. Hewitt, P.J. Fallon, D.R. McKenzie, C.A. Davis, Optical and electronic properties of amorphous diamond. Diam. Relat. Mater. **2**, 782 (1993)
68. I.I. Aksenov, V.A. Belous, V.G. Padalka, V.M. Khoroshikh, Apparatus to rid the plasma of a vacuum arc of macroparticles. Instrum. Exp. Tech. **21**, 1416 (1978)
69. M.M.M. Bilek, A. Anders, Designing advanced filters for macroparticle removal from cathodic arc plasmas. Plasma Sources Sci. Technol. **8**, 488 (1999)
70. A. Anders, W. Fong, A.V. Kulkarni, F.W. Ryan, C.S. Bhatia, Ultrathin diamond-like carbon films deposited by filtered carbon vacuum arcs. IEEE Trans. Plasma Sci. **29**, 768 (2001)
71. D.A. Baldwin, S. Falabella, Deposition processes utilizing a new filtered cathodic arc source. *Proc. 38th Soc. Vacuum Coaters Technol.*, Society of Vacuum Coaters, Albuquerque, NM, pp. 309–316, 1995
72. S. Anders, A. Anders, M.R. Dickinson, R.A. MacGill, I.G. Brown, S-shaped magnetic macroparticle filter for cathodic arc deposition. IEEE Trans. Plasma Sci. **25**, 670 (1997)
73. T. Witke, T. Schuelke, B. Schultrich, P. Siemroth, J. Vetter, Comparison of filtered high-current pulsed arc deposition (φ-HCA) with conventional vacuum arc methods. Surf. Coat. Technol. **126**, 81 (2000)
74. R.P. Welty, Rectangular vacuum-arc plasma source. *U. S. Patent 5,480,527* (1996)
75. V.I. Gorokhovsky, Apparatus for application of coatings in vacuum. *U. S. Patent 5,435,900* (1995)
76. X. Shi, B.K. Tay, H.S. Tan, E. Liu, J. Shi, L.K. Cheah, X. Jin, Transport of vacuum arc plasma through an off-plane double bend filtering duct. Thin Solid Films **345**, 1 (1999)
77. X. Shi, B.K. Tay, S.P. Lau, The double bend filtered cathodic arc technology and its applications. Int. J. Mod. Phys. B **14**, 136 (2000)
78. T. Witke, P. Siemroth, Deposition of droplet-free films by vacuum arc evaporation - results and applications. *IEEE Proc. 18th Int. Symp. on Discharges and Electrical Insulation in Vacuum*, Eindhoven, The Netherlands, pp. 605–608, 1998
79. J. Wei, H. Li, L. Liu, P. Guo, P. Ke, A. Wang, Enhanced tribological and corrosion properties of multilayer ta-C films via alternating sp^3 content. Surf. Coat. Technol. **374**, 317 (2019)
80. A. Anders, Approaches to rid cathodic arc plasmas of macro- and nanoparticles: a review. Surf. Coat. Technol. **120–121**, 319 (1999)
81. J. Matlak, E. Rismaniyazdi, K. Komvopoulos, Nanostructure, structural stability, and diffusion characteristics of layered coatings for heat-assisted magnetic recording head media. Sci. Rep. **8**, 9807 (2018)
82. S. Wang, A. Roy, K. Komvopoulos, Thermal stability and diffusion characteristics of ultrathin amorphous carbon films grown on crystalline and nitrogenated silicon substrates by filtered cathodic vacuum arc deposition. Sci. Rep. **11**, 13106 (2021)
83. X. Chen, Z. Peng, X. Yu, Z. Fu, W. Yue, C. Wang, Microstructure and tribological performance of self-lubricating diamond/tetrahedral amorphous carbon composite film. Appl. Surf. Sci. **257**, 3180 (2011)
84. D. Sheeja, B.K. Tay, C.Q. Sun, Y.Q. Fu, Characterization of Ti-containing amorphous carbon films prepared on titanium substrates. J. Mater. Sci. **38**, 421 (2003)
85. S. Logothetidis, C. Charitidis, P. Patsalas, Engineering properties of fully sp^3- to sp^2-bonded carbon films and their modifications after post-growth ion irradiation. Diam. Relat. Mater. **11**, 1095 (2002)
86. X. Ding, Y.J. Li, Z. Sun, B.K. Tay, S.P. Lau, G.Y. Chen, W. Cheung, S. Wong, Electron field emission from Ti-containing tetrahedral amorphous carbon films deposited by filtered cathodic vacuum arc. J. Appl. Phys. **88**, 6842 (2000)

87. H. Pan, M. Pruski, B.C. Gerstein, F. Li, J.S. Lannin, Local coordination of carbon atoms in amorphous carbon. Phys. Rev. B **44**, 6741 (1991)
88. S. Kaplan, F. Jansen, M. Machonkin, Characterization of amorphous carbon-hydrogen films by solid-state nuclear magnetic resonance. Appl. Phys. Lett. **47**, 750 (1985)
89. M.A. Tamor, W.C. Vassell, K.R. Carduner, Atomic constraint in hydrogenated "diamond-like" carbon. Appl. Phys. Lett. **58**, 592 (1991)
90. A.C. Ferrari, A. Libassi, B.K. Tanner, V. Stolojan, J. Yuan, L.M. Brown, S.E. Rodil, B. Kleinsorge, J. Robertson, Density, sp^3 fraction, and cross-sectional structure of amorphous carbon films determined by x-ray reflectivity and electron energy-loss spectroscopy. Phys. Rev. B **62**, 11089 (2000)
91. C.A. Lucas, T.D. Nguyen, J.B. Kortright, X-ray reflectivity measurements of the expansion of carbon films upon annealing. Appl. Phys. Lett. **59**, 2100 (1991)
92. Q. Zhang, S.F. Yoon, Rusli, J. Ahn, H. Yang, D. Bahr, Deposition of hydrogenated diamond-like carbon films under the impact of energetic hydrocarbon ions. J. Appl. Phys. **84**, 5538 (1998)
93. R.P. Vidano, D.B. Fischbach, L.J. Willis, T.M. Loehr, Observation of Raman band shifting with excitation wavelength for carbons and graphites. Solid State Commun. **39**, 341 (1981)
94. D.S. Knight, W.B. White, Characterization of diamond films by Raman spectroscopy. J. Mater. Res. **4**, 385 (1989)
95. B.S. Elman, M. Shayegan, M.S. Dresselhaus, H. Mazurek, G. Dresselhaus, Structural characterization of ion-implanted graphite. Phys. Rev. B **25**, 4142 (1982)
96. R. Haerle, E. Riedo, A. Pasquarello, A. Baldereschi, sp^2/sp^3 hybridization ratio in amorphous carbon from C 1*s* core-level shifts: X-ray photoelectron spectroscopy and first-principles calculation. Phys. Rev. B **65**, 045101 (2001)
97. N. Wang, K. Komvopoulos, Incidence angle effect of energetic carbon ions on deposition rate, topography, and structure of ultrathin amorphous carbon films deposited by filtered cathodic vacuum arc. IEEE Trans. Magn. **48**, 2220 (2012)
98. J. Xie, K. Komvopoulos, The effect of Argon ion irradiation on the thickness and structure of ultrathin amorphous carbon films. J. Appl. Phys. **119**, 095304 (2016)
99. N. Wang, K. Komvopoulos, The effect of deposition energy of energetic atoms on the growth and structure of ultrathin amorphous carbon films studied by molecular dynamics simulations. J. Phys. D **47**, 245303 (2014)
100. J. Matlak, K. Komvopoulos, Friction properties of amorphous carbon ultrathin films deposited by filtered cathodic vacuum arc and radio-frequency sputtering. Thin Solid Films **579**, 167 (2015)
101. M.P. Siegal, J.C. Barbour, P.N. Provencio, D.R. Tallant, T.A. Friedmann, Amorphous-tetrahedral diamondlike carbon layered structures resulting from film growth energetics. Appl. Phys. Lett. **73**, 759 (1998)
102. P. Kovarik, E.B.D. Bourdon, R.H. Prince, Electron-energy-loss characterization of laser-deposited *a*-C, *a*-C:H, and diamond films. Phys. Rev. B **48**, 12123 (1993)
103. P.J. Fallon, V.S. Veerasamy, C.A. Davis, J. Robertson, G.A.J. Amaratunga, W.I. Milne, J. Koskinen, Properties of filtered-ion-beam-deposited diamondlike carbon as a function of ion energy. Phys. Rev. B **48**, 4777 (1993)
104. R. Lossy, D.L. Pappas, R.A. Roy, J.P. Doyle, J.J. Cuomo, J. Bruley, Properties of amorphous diamond films prepared by a filtered cathodic arc. J. Appl. Phys. **77**, 4750 (1995)
105. S.D. Berger, D.R. McKenzie, P.J. Martin, EELS analysis of vacuum arc-deposited diamond-like films. Philo. Mag. Lett. **57**, 285 (1988)
106. S. Waidmann, M. Knupfer, J. Fink, B. Kleinsorge, J. Robertson, High-resolution electron energy-loss spectroscopy of undoped and nitrogen-doped tetrahedral amorphous carbon films. Diam. Relat. Mater. **9**, 722 (2000)
107. S. Waidmann, M. Knupfer, J. Fink, B. Kleinsorge, J. Robertson, Electronic structure studies of undoped and nitrogen-doped tetrahedral amorphous carbon using high-resolution electron energy-loss spectroscopy. J. Appl. Phys. **89**, 3783 (2001)
108. D. Galvan, Y.T. Pei, J.T.M. De Hosson, A. Cavaleiro, Determination of the sp(3) C content of a-C films through EELS analysis in the TEM. Surf. Coat. Technol. **200**, 739 (2005)
109. J. Robertson, Deposition of diamond-like carbon, in *Thin Film Diamond*, ed. by A.H. Lettington, J.W. Steeds (Springer, Dordrecht, 1994), pp.107–116
110. J. Xie, K. Komvopoulos, Thermal stability of ultrathin amorphous carbon films synthesized by plasma-enhanced chemical vapor deposition and filtered cathodic vacuum arc. Philo. Mag. **97**, 820 (2017)
111. B.K. Pathem, X.-C. Guo, F. Rose, N. Wang, K. Komvopoulos, E. Schreck, B. Marchon, Carbon overcoat oxidation in heat-assisted magnetic recording. IEEE Trans. Magn. **49**, 3721 (2013)
112. N. Wang, K. Komvopoulos, Thermal stability of ultrathin amorphous carbon films for energy-assisted magnetic recording. IEEE Trans. Magn. **47**, 2277 (2011)
113. G.M. Pharr, D.L. Callahan, S.D. McAdams, T.Y. Tsui, S. Anders, A. Anders, J.W. Ager III., I.G. Brown, C.S. Bhatia, S.R.P. Silva, J. Robertson, Hardness, elastic modulus, and structure of very hard carbon films produced by cathodic-arc deposition with substrate pulse biasing. Appl. Phys. Lett. **68**, 779 (1996)
114. E. Martınez, J.L. Andújar, M.C. Polo, J. Esteve, J. Robertson, W.I. Milne, Study of the mechanical properties of tetrahedral amorphous carbon films by nanoindentation and nanowear measurements. Diam. Relat. Mater. **10**, 145 (2001)
115. M. Chhowalla, J. Robertson, C.W. Chen, S.R.P. Silva, C.A. Davis, G.A.J. Amaratunga, W.I. Milne, Influence of ion energy and substrate temperature on the optical and electronic properties

of tetrahedral amorphous carbon (*ta*-C) films. J. Appl. Phys. **81**, 139 (1997)
116. S. Sattel, J. Robertson, H. Ehrhardt, Effects of deposition temperature on the properties of hydrogenated tetrahedral amorphous carbon. J. Appl. Phys. **82**, 4566 (1997)
117. J. Wei, P. Guo, L. Liu, H. Li, H. Li, S. Wang, P. Ke, A. Wang, Tailored electrochemical behavior of ta-C film by glancing angle deposition. Appl. Surf. Sci. **516**, 146115 (2020)
118. D. Sheeja, B.K. Tay, S.P. Lau, X. Shi, Tribological properties and adhesive strength of DLC coatings prepared under different substrate bias voltages. Wear **249**, 433 (2001)
119. N. Dwivedi, R.J. Yeo, Z. Zhang, C. Dhand, S. Tripathy, C.S. Bhatia, Direct observation of thickness and foreign interlayer driven abrupt structural transformation in ultrathin carbon and hybrid silicon nitride/carbon films. Carbon **115**, 701 (2017)
120. N. Dwivedi, E. Rismani-Yazdi, R.J. Yeo, P.S. Goohpattader, N. Satyanarayana, N. Srinivasan, B. Druz, S. Tripathy, C.S. Bhatia, Probing the role of an atomically thin SiN_x interlayer on the structure of ultrathin carbon films. Sci. Rep. **4**, 5021 (2014)
121. N. Dwivedi, R.J. Yeo, C. Dhand, J. Risan, R. Nay, S. Tripathy, S. Rajauria, M.S.M. Saifullah, S.K.R.S. Sankaranarayanan, H. Yang, A. Danner, C.S. Bhatia, Boosting contact sliding and wear protection via atomic intermixing and tailoring of nanoscale interfaces. Sci. Adv. **5**, eaau7886 (2019)
122. R.J. Yeo, N. Dwivedi, L. Zhang, Z. Zhang, C.Y.H. Lim, S. Tripathy, C.S. Bhatia, Superior wear resistance and low friction in hybrid ultrathin silicon nitride/carbon films: synergy of the interfacial chemistry and carbon microstructure. Nanoscale **9**, 14937 (2017)
123. G.-G. Wang, X.-P. Kuang, H.-Y. Zhang, C. Zhu, J.-C. Han, H.-B. Zuo, H.-T. Ma, Silicon nitride gradient film as the underlayer of ultra-thin tetrahedral amorphous carbon overcoat for magnetic recording slider. Mater. Chem. Phys. **131**, 127 (2011)
124. N. Dwivedi, R.J. Yeo, Z. Zhang, C. Dhand, S. Tripathy, C.S. Bhatia, Interface engineering and controlling the friction and wear of ultrathin carbon films: high sp^3 versus high sp^2 carbons. Adv. Funct. Mater. **26**, 1526 (2016)
125. R.J. Yeo, N. Dwivedi, S. Tripathy, C.S. Bhatia, Excellent wear life of silicon nitride/tetrahedral amorphous carbon bilayer overcoat on functional tape heads. Appl. Phys. Lett. **106**, 091604 (2015)
126. R.J. Yeo, N. Dwivedi, E. Rismani, N. Satyanarayana, S. Kundu, P.S. Goohpattader, H.R. Tan, N. Srinivasan, B. Druz, S. Tripathy, C.S. Bhatia, Enhanced tribological, corrosion, and microstructural properties of an ultrathin (<2 nm) silicon nitride/carbon bilayer overcoat for high density magnetic storage. ACS Appl. Mater. Interfaces **6**, 9376 (2014)
127. I. Alexandrou, H.-J. Scheibe, C.J. Kiely, A.J. Papworth, G.A.J. Amaratunga, B. Schultrich, Carbon films with an sp^2 network structure. Phys. Rev. B **60**, 10903 (1999)
128. N. Dwivedi, N. Satyanarayana, R.J. Yeo, H. Xu, K.P. Loh, S. Tripathy, C.S. Bhatia, Ultrathin carbon with interspersed graphene/fullerene-like nanostructures: a durable protective overcoat for high density magnetic storage. Sci. Rep. **5**, 11607 (2015)
129. J.T. Gudmundsson, A. Anders, A. von Keudell, Foundations of physical vapor deposition with plasma assistance. Plasma Sources Sci. Technol. **31**, 083001 (2022)
130. J.H. Keller, W.B. Pennebaker, Electrical properties of RF sputtering systems. IBM J. Res. Dev. **23**, 3 (1979)
131. D. Wan, K. Komvopoulos, Effect of low-pressure plasma discharge conditions on the thickness and roughness of ultrathin films of amorphous carbon. J. Appl. Phys. **100**, 063307 (2006)
132. J.W. Coburn, E. Kay, Positive-ion bombardment of substrates in rf diode glow discharge sputtering. J. Appl. Phys. **43**, 4965 (1972)
133. J. Xie, K. Komvopoulos, Hybridization and tribomechanical properties of ultrathin amorphous carbon films synthesized by radio-frequency low-pressure plasma discharges. Surf. Coat. Technol. **262**, 15 (2015)
134. D. Wan, K. Komvopoulos, Probabilistic analysis of tetrahedral carbon hybridization in amorphous carbon films. Appl. Phys. Lett. **88**, 221908 (2006)
135. D. Wan, K. Komvopoulos, Formation of diamondlike nanocrystallites in amorphous carbon films synthesized by radio-frequency sputtering. J. Mater. Res. **23**, 700 (2008)
136. J. Xie, K. Komvopoulos, Friction, nanostructure, and residual stress of single-layer and multi-layer amorphous carbon films deposited by radio-frequency sputtering. J. Mater. Res. **31**, 1857 (2016)
137. W. Lu, K. Komvopoulos, Implanted argon atoms as sensing probes of residual stress in ultrathin films. Appl. Phys. Lett. **76**, 3206 (2000)
138. W. Lu, K. Komvopoulos, P. Patsalas, C. Charitidis, M. Gioti, S. Logothetidis, Microstructure and nanomechanical and optical properties of single- and multi-layer carbon films synthesized by radio frequency sputtering. Surf. Coat. Technol. **168**, 12 (2003)
139. W. Lu, K. Komvopoulos, Microstructure and nanomechanical properties of nitrogenated amorphous carbon thin films synthesized by reactive radio frequency sputtering. J. Appl. Phys. **85**, 2642 (1999)
140. B.K. Gupta, B. Bhushan, Mechanical and tribological properties of hard carbon coatings for magnetic recording heads. Wear **190**, 110 (1995)
141. N. Savvides, B. Window, Diamondlike amorphous carbon films prepared by magnetron sputtering of graphite. J. Vac. Sci. Technol. A **3**, 2386 (1985)
142. R. Kleber, M. Weiler, A. Krüger, S. Sattel, G. Kunz, K. Jung, H. Ehrhardt, Influence of ion energy and flux composition on the properties of plasma-deposited amorphous carbon and

amorphous hydrogenated carbon films. Diam. Relat. Mater. **2**, 246 (1993)
143. N.A. Sánchez, C. Rincón, G. Zambrano, H. Galindo, P. Prieto, Characterization of diamond-like carbon (DLC) thin films prepared by r.f. magnetron sputtering. Thin Solid Films **373**, 247 (2000)
144. V. Kouznetsov, K. Macák, J.M. Schneider, U. Helmersson, I. Petrov, A novel pulsed magnetron sputter technique utilizing very high target power densities. Surf. Coat. Technol. **122**, 290 (1999)
145. B. André, F. Rossi, H. Dunlop, Ion beam assisted growth of dense diamond-like carbon. Diam. Relat. Mater. **1**, 307 (1992)
146. J. Vlček, K. Rusňák, V. Hájek, L. Martinů, Reactive magnetron sputtering of CN_x films: ion bombardment effects and process characterization using optical emission spectroscopy. J. Appl. Phys. **86**, 3646 (1999)
147. N. Hellgren, M.P. Johansson, E. Broitman, P. Sandström, L. Hultman, J.-E. Sundgren, Effect of chemical sputtering on the growth and structural evolution of magnetron sputtered CN_x thin films. Thin Solid Films **382**, 146 (2001)
148. R. Kaltofen, T. Sebald, G. Weise, Plasma diagnostic studies to the carbon nitride film deposition by reactive r.f. magnetron sputtering. Thin Solid Films **290**, 112 (1996)
149. N. Hellgren, M.P. Johansson, E. Broitman, L. Hultman, J.-E. Sundgren, Role of nitrogen in the formation of hard and elastic CN_x thin films by reactive magnetron sputtering. Phys. Rev. B **59**, 5162 (1999)
150. J. Schwan, S. Ulrich, H. Roth, H. Ehrhardt, S.R.P. Silva, J. Robertson, R. Samlenski, R. Brenn, Tetrahedral amorphous carbon films prepared by magnetron sputtering and dc ion plating. J. Appl. Phys. **79**, 1416 (1996)
151. S. Kundu, N. Dwivedi, N. Satyanarayana, R.J. Yeo, J. Ahner, P.M. Jones, C.S. Bhatia, Probing the role of carbon microstructure on the thermal stability and performance of ultrathin (<2 nm) overcoats on L_{10} FePt media for heat-assisted magnetic recording. ACS Appl. Mater. Interfaces **7**, 158 (2015)
152. J.J. Cuomo, J.P. Doyle, J. Bruley, J.C. Liu, Sputter deposition of dense diamond-like carbon films at low temperature. Appl. Phys. Lett. **58**, 466 (1991)
153. F. Davanloo, E.M. Juengerman, D.R. Jander, T.J. Lee, C.B. Collins, Laser plasma diamond. J. Mater. Res. **5**, 2398 (1990)
154. S. Bhargava, H.D. Bist, S.B. Samanta, A.V. Narlikar, A. Rengan, J. Narayan, Nanoclusters in laser ablated diamond-like carbon films through scanning tunneling microscopy. Solid State Commun. **90**, 205 (1994)
155. E.B.D. Bourdon, W.W. Duley, A.P. Jones, R.H. Prince, Characterization of diamond-like films prepared by laser ablation of graphite. Surf. Coat. Technol. **47**, 509 (1991)
156. D.L. Pappas, K.L. Saenger, J. Bruley, W. Krakow, J.J. Cuomo, T. Gu, R.W. Collins, Pulsed laser deposition of diamond-like carbon films. J. Appl. Phys. **71**, 5675 (1992)
157. J. Cheung, J. Horwitz, Pulsed laser deposition history and laser-target interactions. MRS Bull. **17**, 30 (1992)
158. F. Müller, K. Mann, Laser-induced physical vapour deposition of diamond-like carbon films. Diam. Relat. Mater. **2**, 233 (1993)
159. C. Germain, C. Girault, R. Gisbert, J. Aubreton, A. Catherinot, KrF laser photo-ablation of a graphite target: application to the development of thin films. Diam. Relat. Mater. **3**, 598 (1994)
160. J. Karpman, M. Riabkina-Fishman, J. Zahavi, D. Dhamelincourt, Properties of unhydrogenated diamond-like carbon films deposited by ArF excimer laser. Diam. Relat. Mater. **4**, 10 (1994)
161. V.I. Merkulov, D.H. Lowndes, G.E. Jellison Jr., A.A. Puretzky, D.B. Geohegan, Structure and optical properties of amorphous diamond films prepared by ArF laser ablation as a function of carbon ion kinetic energy. Appl. Phys. Lett. **73**, 2591 (1998)
162. J.J. Cuomo, D.L. Pappas, J. Bruley, J.P. Doyle, K.L. Saenger, Vapor deposition processes for amorphous carbon films with sp^3 fractions approaching diamond. J. Appl. Phys. **70**, 1706 (1991)
163. J. Krishnaswamy, A. Rengan, J. Narayan, K. Vedam, C.J. McHargue, Thin-film deposition by a new laser ablation and plasma hybrid technique. Appl. Phys. Lett. **54**, 2455 (1989)
164. C.B. Collins, F. Davanloo, E.M. Juengerman, W.R. Osborn, D.R. Jander, Laser plasma source of amorphic diamond. Appl. Phys. Lett. **54**, 216 (1989)
165. S.S. Wagal, E.M. Juengerman, C.B. Collins, Diamond-like carbon films prepared with a laser ion source. Appl. Phys. Lett. **53**, 187 (1988)
166. J.A. Greer, M.D. Tabat, Large-area pulsed laser deposition: techniques and applications. J. Vac. Sci. Technol. A **13**, 1175 (1995)
167. S.F. Yoon, K.H. Tan, Rusli, J. Ahn, Q.F. Huang, Comparative study on the effects of ion density and ion energy on diamond-like carbon deposited by electron cyclotron resonance chemical vapor deposition. J. Appl. Phys. **89**, 4830 (2001)
168. M.K. Fung, W.C. Chan, K.H. Lai, I. Bello, C.S. Lee, N.B. Wong, S.T. Lee, Deposition of ultra-thin diamond-like carbon protective coating on magnetic disks by electron cyclotron resonance plasma technique. J. Non-Cryst. Solids **254**, 167 (1999)
169. A. Grill, V. Patel, B.S. Meyerson, Optical and tribological properties of heat-treated diamond-like carbon. J. Mater. Res. **5**, 2531 (1990)
170. A. Grill, B. Meyerson, V. Patel, Interface modifications for improving the adhesion of *a*-C:H films to metals. J. Mater. Res. **3**, 214 (1988)
171. Ishpal, S. Kumar, N. Dwivedi, C.M.S. Rauthan, Investigation of radio frequency plasma for the growth of diamond like carbon films. Phys. Plasmas **19**, 033515 (2012)
172. N. Dwivedi, S. Kumar, I. Rawal, H.K. Malik, Influence of consumed power on structural and nano-mechanical properties of nano-structured diamond-like carbon thin films. Appl. Surf. Sci. **300**, 141 (2014)
173. B. Bhushan, A.J. Kellock, N.-H. Cho, J.W. Ager III, Characterization of chemical bonding and physical characteristics of

diamond-like amorphous carbon and diamond films. J. Mater. Res. **7**, 404 (1992)
174. E. Bertran, F.J. Pino, G. Viera, J.L. Andújar, Hard coatings for mechanical applications. Vacuum **64**, 181 (2002)
175. Y. Catherine, P. Couderc, Electrical characteristics and growth kinetics in discharges used for plasma deposition of amorphous carbon. Thin Solid Films **144**, 265 (1986)
176. G.J. Vandentop, M. Kawasaki, R.M. Nix, I.G. Brown, M. Salmeron, G.A. Somorjai, Formation of hydrogenated amorphous carbon films of controlled hardness from a methane plasma. Phys. Rev. B **41**, 3200 (1990)
177. P.M. Jones, J. Ahner, C.L. Platt, H. Tang, J. Hohlfeld, Understanding disk carbon loss kinetics for heat assisted magnetic recording. IEEE Trans. Magn. **50**, 144 (2014)
178. J.R. Conrad, J.L. Radtke, R.A. Dodd, F.J. Worzala, N.C. Tran, Plasma source ion-implantation technique for surface modification of materials. J. Appl. Phys. **62**, 4591 (1987)
179. J.R. Conrad, Plasma source ion implantation: a new approach to ion beam modification of materials. Mater. Sci. Eng. A **116**, 197 (1989)
180. I.G. Brown, A. Anders, S. Anders, M.R. Dickinson, I.C. Ivanov, R.A. MacGill, X.Y. Yao, K.-M. Yu, Plasma synthesis of metallic and composite thin films with atomically mixed substrate bonding. Nucl. Instrum. Meth. Phys. Res. B **80–81**, 1281 (1993)
181. I.G. Brown, A. Anders, S. Anders, M.R. Dickinson, R.A. MacGill, Metal ion implantation: conventional versus immersion. J. Vac. Sci. Technol. B **12**, 823 (1994)
182. P.K. Chu, B.Y. Tang, L.P. Wang, X.F. Wang, S.Y. Wang, N. Huang, Third-generation plasma immersion ion implanter for biomedical materials and research. Rev. Sci. Instrum. **72**, 1660 (2001)
183. K. Komvopoulos, B. Wei, S. Anders, A. Anders, I.G. Brown, Surface modification of magnetic recording heads by plasma immersion ion implantation and deposition. J. Appl. Phys. **76**, 1656 (1994)
184. D.H. Lee, X.M. He, K.C. Walter, M. Nastasi, J.R. Tesmer, M. Tuszewski, D.R. Tallant, Diamondlike carbon deposition on silicon using radio-frequency inductive plasma of Ar and C_2H_2 gas mixture in plasma immersion ion deposition. Appl. Phys. Lett. **73**, 2423 (1998)
185. D.H. Lee, S. Fayeulle, K.C. Walter, M. Nastasi, Internal stress reduction in diamond like carbon thin films by ion irradiation. Nucl. Instrum. Meth. Phys. Res. B **148**, 216 (1999)
186. S. Anders, A. Anders, I.G. Brown, B. Wei, K. Komvopoulos, J.W. Ager III, K.M. Yu, Effect of vacuum arc deposition parameters on the properties of amorphous carbon thin films. Surf. Coat. Technol. **68–69**, 388 (1994)
187. B. Wei, K. Komvopoulos, I.G. Brown, Microstructure modification of amorphous carbon films by ion-implantation techniques. J. Mater. Res. **14**, 2181 (1999)
188. K. Komvopoulos, I.G. Brown, B. Wei, S. Anders, A. Anders, C.S. Bhatia, Surface treatment of magnetic recording heads. *U. S. Patent 5,476,691* (1995)
189. K. Komvopoulos, I.G. Brown, B. Wei, S. Anders, A. Anders, C.S. Bhatia, Surface treatment of magnetic recording heads. *U. S. Patent 5,838,522* (1998)
190. I.G. Brown, X. Godechot, K.M. Yu, Novel metal ion surface modification technique. Appl. Phys. Lett. **58**, 1392 (1991)
191. A. Anders, S. Anders, I.G. Brown, M.R. Dickinson, R.A. MacGill, Metal plasma immersion ion implantation and deposition using vacuum arc plasma sources. J. Vac. Sci. Technol. B **12**, 815 (1994)
192. A. Anders, Metal plasma immersion ion implantation and deposition: a review. Surf. Coat. Technol. **93**, 158 (1997)
193. J. Tendys, I.J. Donnelly, M.J. Kenny, J.T.A. Pollock, Plasma immersion ion implantation using plasmas generated by radio frequency techniques. Appl. Phys. Lett. **53**, 2143 (1988)
194. A. Anders, S. Anders, I.G. Brown, I.C. Ivanov, Low energy ion implantation/deposition as a film synthesis and bonding tool. MRS Proc. **316**, 833 (1993)
195. J. Koskinen, Abrasive wear resistance of ion-deposited hard-carbon films as a function of deposition energy. J. Appl. Phys. **63**, 2094 (1988)
196. B. Schultrich, *Tetrahedrally Bonded Amorphous Carbon Films I: Basics, Structure and Preparation* (Springer-Verlag, Berlin, 2018)
197. S. Ravi, P. Silva, S. Xu, B.X. Tay, H.S. Tan, W.I. Milne, Nanocrystallites in tetrahedral amorphous carbon films. Appl. Phys. Lett. **69**, 491 (1996)
198. W.D. Davis, H.C. Miller, Analysis of the electrode products emitted by dc arcs in a vacuum ambient. J. Appl. Phys. **40**, 2212 (1969)
199. I.I. Aksenov, V.A. Belous, V.G. Padalka, V.M. Khoroshikh, Transport of plasma streams in a curvilinear plasma-optics system. Sov. J. Plasma Phys. **4**, 425 (1978)
200. J. R. Treglio, Magnetically-filtered cathodic arc plasma apparatus. *U. S. Patent 5,317,235* (1994)
201. A. Anders, S. Anders, I.G. Brown, Transport of vacuum arc plasmas through magnetic macroparticle filters. Plasma Sources Sci. Technol. **4**, 1 (1995)
202. A. Anders, S. Anders, I.G. Brown, Effect of duct bias on transport of vacuum arc plasmas through curved magnetic filters. J. Appl. Phys. **75**, 4900 (1994)
203. J.W. Ager III, S. Anders, A. Anders, B. Wei, X.Y. Yao, I.G. Brown, C.S. Bhatia, K. Komvopoulos, Ion implantation post-processing of amorphous carbon films. Diam. Relat. Mater. **8**, 451 (1999)
204. A. Anders, R.A. MacGill, Twist filter for the removal of macroparticles from cathodic arc plasmas. Surf. Coat. Technol. **133–134**, 96 (2000)
205. E. Rismani, S.K. Sinha, S. Tripathy, H. Yang, C.S. Bhatia, Effect of pre-treatment of the substrate surface by energetic C^+ ion

bombardment on structure and nano-tribological characteristics of ultra-thin tetrahedral amorphous carbon (ta-C) protective coatings. J. Phys. D **44**, 115502 (2011)
206. J. Matlak, *Synthesis and characterization of amorphous carbon films for heat-assisted magnetic storage*, PhD Thesis, Department of Mechanical Engineering, University of California, Berkeley, CA (2017)
207. E. Rismani, S.K. Sinha, H. Yang, C.S. Bhatia, Effect of pretreatment of Si interlayer by energetic C^+ ions on the improved nanotribological properties of magnetic head overcoat. J. Appl. Phys. **111**, 084902 (2012)
208. A. Anders, R.A. MacGill, T.A. McVeigh, Efficient, compact power supply for repetitively pulsed, "triggerless" cathodic arcs. Rev. Sci. Instrum. **70**, 4532 (1999)
209. A. Anders, I.G. Brown, R.A. MacGill, M.R. Dickinson, 'Triggerless' triggering of vacuum arcs. J. Phys. D **31**, 584 (1998)
210. A. Anders, J. Schein, N. Qi, Pulsed vacuum-arc ion source operated with a "triggerless" arc initiation method. Rev. Sci. Instrum. **71**, 827 (2000)
211. V.S. Veerasamy, *Tetrahedral amorphous carbon: deposition, characterisation and electronic properties*, PhD Thesis, Department of Materials Science and Metallurgy, University of Cambridge, Cambridge, UK (1994)
212. E. Findeisen, R. Feidenhans'l, M.E. Vigild, K.N. Clausen, J.B. Hansen, M.D. Bentzon, J.P. Goff, Hydrogen concentration and mass density of diamondlike carbon films obtained by x-ray and neutron reflectivity. J. Appl. Phys. **76**, 4636 (1994)
213. M.P. Siegal, D.R. Tallant, L.J. Martinez-Miranda, J.C. Barbour, R.L. Simpson, D.L. Overmyer, Nanostructural characterization of amorphous diamondlike carbon films. Phys. Rev. B **61**, 10451 (2000)
214. P.E. Kondrashov, I.S. Smirnov, Y.E. Lukashov, S.Y. Yablokov, A.M. Baranov, D.P. Dowling, K. Donnelly, R.V. Flood, M.L. McConnell, Investigation of ultrathin DLC film growth by a novel X-ray reflectivity technique and in situ ellipsometry. Diam. Relat. Mater. **8**, 532 (1999)
215. S. Logothetidis, G. Stergioudis, Studies of density and surface roughness of ultrathin amorphous carbon films with regards to thickness with x-ray reflectometry and spectroscopic ellipsometry. Appl. Phys. Lett. **71**, 2463 (1997)
216. M.G. Beghi, A.C. Ferrari, K.B.K. Teo, J. Robertson, C.E. Bottani, A. Libassi, B.K. Tanner, Bonding and mechanical properties of ultrathin diamond-like carbon films. Appl. Phys. Lett. **81**, 3804 (2002)
217. M.C. Polo, J.L. Andújar, A. Hart, J. Robertson, W.I. Milne, Preparation of tetrahedral amorphous carbon films by filtered cathodic vacuum arc deposition. Diam. Relat. Mater. **9**, 663 (2000)
218. S.S. Roy, R. McCann, P. Papakonstantinou, P. Maguire, J.A. McLaughlin, The structure of amorphous carbon nitride films using a combined study of NEXAFS, XPS and Raman spectroscopies. Thin Solid Films **482**, 145 (2005)
219. S.S. Roy, P. Papakonstantinou, R. McCann, G. Abbas, J.P. Quinn, J. McLaughlin, Bonding configurations in DBOP-FCVA nitrogenated tetrahedral amorphous carbon films studied by Raman and X-ray photoelectron spectroscopies. Diam. Relat. Mater. **13**, 1459 (2004)
220. C.K. Park, S.M. Chang, H.S. Uhm, S.H. Seo, J.S. Park, XPS and XRR studies on microstructures and interfaces of DLC films deposited by FCVA method. Thin Solid Films **420–421**, 235 (2002)
221. O.S. Panwar, Y. Aparna, S.M. Shivaprasad, M.A. Khan, B.S. Satyanarayana, R. Bhattacharyya, XPS and XAES studies of as grown and nitrogen incorporated tetrahedral amorphous carbon films deposited by pulsed unfiltered cathodic vacuum arc process. Appl. Surf. Sci. **221**, 392 (2004)
222. B.K. Tay, X. Shi, H.S. Tan, D.H.C. Chua, Investigation of tetrahedral amorphous carbon films using x-ray photoelectron and Raman spectroscopy. Surf. Interface Anal. **28**, 231 (1999)
223. P. Patsalas, S. Logothetidis, S. Kennou, C. Gravalidis, Surface-activation processes and ion–solid interactions during the nucleation and growth of ultra-thin amorphous carbon films. Thin Solid Films **428**, 211 (2003)
224. A.C. Ferrari, J. Robertson, Raman spectroscopy of amorphous, nanostructured, diamond–like carbon, and nanodiamond. Philo. Trans. R. Soc. Lond. **362**, 2477 (2004)
225. A.C. Ferrari, J. Robertson, Resonant Raman spectroscopy of disordered, amorphous, and diamondlike carbon. Phys. Rev. B **64**, 075414 (2001)
226. A.C. Ferrari, J. Robertson, Interpretation of Raman spectra of disordered and amorphous carbon. Phys. Rev. B **61**, 14095 (2000)
227. S. Prawer, K.W. Nugent, Y. Lifshitz, G.D. Lempert, E. Grossman, J. Kulik, I. Avigal, R. Kalish, Systematic variation of the Raman spectra of DLC films as a function of sp^2:sp^3 composition. Diam. Relat. Mater. **5**, 433 (1996)
228. S. Xu, D. Flynn, B.K. Tay, S. Prawer, K.W. Nugent, S.R.P. Silva, Y. Lifshitz, W.I. Milne, Mechanical properties and Raman spectra of tetrahedral amorphous carbon films with high sp^3 fraction deposited using a filtered cathodic arc. Philo. Mag. B **76**, 351 (1997)
229. R.F. Egerton, *Electron Energy-Loss Spectroscopy in the Electron Microscope*, 3rd edn. (Springer, New York, 2011)
230. C.W. Tan, S. Maziar, E.H.T. Teo, B.K. Tay, Microstructure and through-film electrical characteristics of vertically aligned amorphous carbon films. Diam. Relat. Mater. **20**, 290 (2011)
231. Y. Lifshitz, S.R. Kasi, J.W. Rabalais, W. Eckstein, Subplantation model for film growth from hyperthermal species. Phys. Rev. B **41**, 10468 (1990)
232. J. Xie, K. Komvopoulos, Bilayer amorphous carbon films synthesized by filtered cathodic vacuum arc deposition. J. Mater. Res. **31**, 3161 (2016)

233. M.M. Golzan, P.B. Lukins, D.R. McKenzie, A.M. Vassallo, J.V. Hanna, NMR evidence for strained carbon bonding in tetrahedral amorphous carbon. Chem. Phys. **193**, 167 (1995)
234. R.H. Jarman, G.J. Ray, R.W. Standley, G.W. Zajac, Determination of bonding in amorphous carbon films: a quantitative comparison of core-electron energy-loss spectroscopy and ^{13}C nuclear magnetic resonance spectroscopy. Appl. Phys. Lett. **49**, 1065 (1986)
235. R. Kleber, K. Jung, H. Ehrhardt, I. Mühling, K. Breuer, H. Metz, F. Engelke, Characterization of the sp^2 bonds network in a-C:H layers with nuclear magnetic resonance, electron energy loss spectroscopy and electron spin resonance. Thin Solid Films **205**, 274 (1991)
236. C. Jäger, J. Gottwald, H.W. Spiess, R.J. Newport, Structural properties of amorphous hydrogenated carbon. III. NMR investigations. Phys. Rev. B **50**, 846 (1994)
237. A. Grill, B.S. Meyerson, V.V. Patel, J.A. Reimer, M.A. Petrich, Inhomogeneous carbon bonding in hydrogenated amorphous carbon films. J. Appl. Phys. **61**, 2874 (1987)
238. C. Donnet, J. Fontaine, F. Lefèbvre, A. Grill, V. Patel, C. Jahnes, Solid state ^{13}C and ^{1}H nuclear magnetic resonance investigations of hydrogenated amorphous carbon. J. Appl. Phys. **85**, 3264 (1999)
239. J.J. Cuomo, D.L. Pappas, R. Lossy, J.P. Doyle, J. Bruley, G.W. Di Bello, W. Krakow, Energetic carbon deposition at oblique angles. J. Vac. Sci. Technol. A **10**, 3414 (1992)
240. D. Liu, G. Benstetter, E. Lodermeier, J. Vancea, Influence of the incident angle of energetic carbon ions on the properties of tetrahedral amorphous carbon (ta-C) films. J. Vac. Sci. Technol. A **21**, 1665 (2003)
241. F.-X. Liu, K.-L. Yao, Z.-L. Liu, Substrate tilting effect on structure of tetrahedral amorphous carbon films by Raman spectroscopy. Surf. Coat. Technol. **201**, 7235 (2007)
242. D. Sheeja, B.K. Tay, J.Y. Sze, L.J. Yu, S.P. Lau, A comparative study between pure and Al-containing amorphous carbon films prepared by FCVA technique together with high substrate pulse biasing. Diam. Relat. Mater. **12**, 2032 (2003)
243. P.R. Poudel, P.P. Poudel, B. Rout, M. ElBouanani, F.D. McDaniel, An XPS study to investigate the dependence of carbon ion fluences in the formation of buried SiC. Nucl. Instrum. Meth. Phys. Res. B **283**, 93 (2012)
244. T. Kamwanna, N. Pasaja, L.D. Yu, T. Vilaithong, A. Anders, S. Singkarat, MeV-ion beam analysis of the interface between filtered cathodic arc-deposited *a*-carbon and single crystalline silicon. Nucl. Instrum. Meth. Phys. Res. B **266**, 5175 (2008)
245. R.L.C. Wu, K. Miyoshi, R. Vuppuladhadium, H.E. Jackson, Physical and tribological properties of rapid thermal annealed diamond-like carbon films. Surf. Coat. Technol. **54–55**, 576 (1992)
246. A.C. Ferrari, B. Kleinsorge, N.A. Morrison, A. Hart, V. Stolojan, J. Robertson, Stress reduction and bond stability during thermal annealing of tetrahedral amorphous carbon. J. Appl. Phys. **85**, 7191 (1999)
247. S. Anders, J. Diaz, J.W. Ager III, R.Y. Lo, D.B. Bogy, Thermal stability of amorphous hard carbon films produced by cathodic arc deposition. Appl. Phys. Lett. **71**, 3367 (1997)
248. J. Díaz, S. Anders, X. Zhou, E.J. Moler, S.A. Kellar, Z. Hussain, Combined near edge X-ray absorption fine structure and X-ray photoemission spectroscopies for the study of amorphous carbon thin films. J. Elec. Spectrosc. Relat. Phenom. **101–103**, 545 (1999)
249. D.G. McCulloch, X.L. Xiao, J.L. Peng, P.C.T. Ha, D.R. McKenzie, M.M.M. Bilek, S.P. Lau, D. Sheeja, B.K. Tay, The structure and annealing properties of multilayer carbon films. Surf. Coat. Technol. **198**, 217 (2005)
250. S. Wang, K. Komvopoulos, Structure evolution during deposition and thermal annealing of amorphous carbon ultrathin films investigated by molecular dynamics simulations. Sci. Rep. **10**, 8089 (2020)
251. B.K. Tay, X. Shi, E.J. Liu, H.S. Tan, L.K. Cheah, W.I. Milne, Heat treatment of tetrahedral amorphous carbon films grown by filtered cathodic vacuum-arc technique. Diam. Relat. Mater. **8**, 1328 (1999)
252. M. Chhowalla, A.C. Ferrari, J. Robertson, G.A.J. Amaratunga, Evolution of sp^2 bonding with deposition temperature in tetrahedral amorphous carbon studied by Raman spectroscopy. Appl. Phys. Lett. **76**, 1419 (2000)
253. N. Tagawa, H. Tani, Lubricant depletion characteristics induced by rapid laser heating in thermally assisted magnetic recording. IEEE Trans. Magn. **47**, 105 (2010)
254. N. Wang, K. Komvopoulos, F. Rose, B. Marchon, Structural stability of hydrogenated amorphous carbon overcoats used in heat-assisted magnetic recording investigated by rapid thermal annealing. J. Appl. Phys. **113**, 083517 (2013)
255. N. Tagawa, H. Tani, Structural stability of nanometer thick diamond-like carbon films subjected to heating for thermally assisted magnetic recording. Microsyst. Technol. **20**, 1405 (2014)
256. S. Wang, Y. Wu, K. Komvopoulos, Single-step metal-catalyzed synthesis of hybrid planar graphene–orbicular graphitic carbon structures using an amorphous carbon thin film as a precursor. Appl. Surf. Sci. **552**, 149018 (2021)
257. O. Penkov, H.-J. Kim, H.-J. Kim, D.-E. Kim, Tribology of graphene: a review. Int. J. Precis. Eng. Manuf. **15**, 577 (2014)
258. N. Dwivedi, A.K. Ott, K. Sasikumar, C. Dou, R.J. Yeo, B. Narayanan, U. Sassi, D. De Fazio, G. Soavi, T. Dutta, O. Balci, S. Shinde, J. Zhang, A.K. Katiyar, P.S. Keatley, A.K. Srivastava, S.K.R.S. Sankaranarayanan, A.C. Ferrari, C.S. Bhatia, Graphene overcoats for ultra-high storage density magnetic media. Nat. Commun. **12**, 2854 (2021)
259. P. Philipp, L. Bischoff, B. Schmidt, Taming of Ga droplets on DLC layers—size tuning and local arrangement with nanometer accuracy. Nanotechnology **23**, 475304 (2012)

260. G.A.J. Amaratunga, M. Chhowalla, C.J. Kiely, I. Alexandrou, R. Aharonov, R.M. Devenish, Hard elastic carbon thin films from linking of carbon nanoparticles. Nature **383**, 321 (1996)
261. Y. Cheng, E.F. Rejda, A.J. Boyne, K.W. Wierman, M. Seigler, S. Franzen, J. Gong, Devices including metal layer. *U. S. Patent Application 2019/0164571 A1* (2019)
262. N. Dwivedi, R.J. Yeo, L.J.K. Yak, N. Satyanarayana, C. Dhand, T.N. Bhat, Z. Zhang, S. Tripathy, C.S. Bhatia, Atomic scale interface manipulation, structural engineering, and their impact on ultrathin carbon films in controlling wear, friction, and corrosion. ACS Appl. Mater. Interfaces **8**, 17606 (2016)
263. E. Rismani, S.K. Sinha, H. Yang, S. Tripathy, C.S. Bhatia, Development of a ta-C wear resistant coating with composite interlayer for recording heads of magnetic tape drives. Tribol. Lett. **46**, 221 (2012)
264. R.J. Yeo, E. Rismani, N. Dwivedi, D.J. Blackwood, H.R. Tan, Z. Zhang, S. Tripathy, C.S. Bhatia, Bi-level surface modification of hard disk media by carbon using filtered cathodic vacuum arc: reduced overcoat thickness without reduced corrosion performance. Diam. Relat. Mater. **44**, 100 (2014)
265. M. Bellardita, A. Di Paola, S. Yurdakal, L. Palmisano, Preparation of catalysts and photocatalysts used for similar processes, in *Heterogeneous Photocatalysis: Relationships with Heterogeneous Catalysts and Perspectives*, ed. by G. Marcì, L. Palmisano (Elsevier, Amsterdam, 2019), pp.25–56
266. K. Gupta, N.K. Jain, R. Laubscher, *Advanced Gear Manufacturing and Finishing: Classical and Modern Processes* (Academic Press, London, 2017), pp.167–196
267. E. Kosobrodova, A. Kondyurin, W. Chrzanowski, C. Theodoropoulos, E. Morganti, D. Hutmacher, M.M.M. Bilek, Effect of plasma immersion ion implantation on polycaprolactone with various molecular weights and crystallinity. J. Mater. Sci. Mater. Med. **29**, 5 (2018)